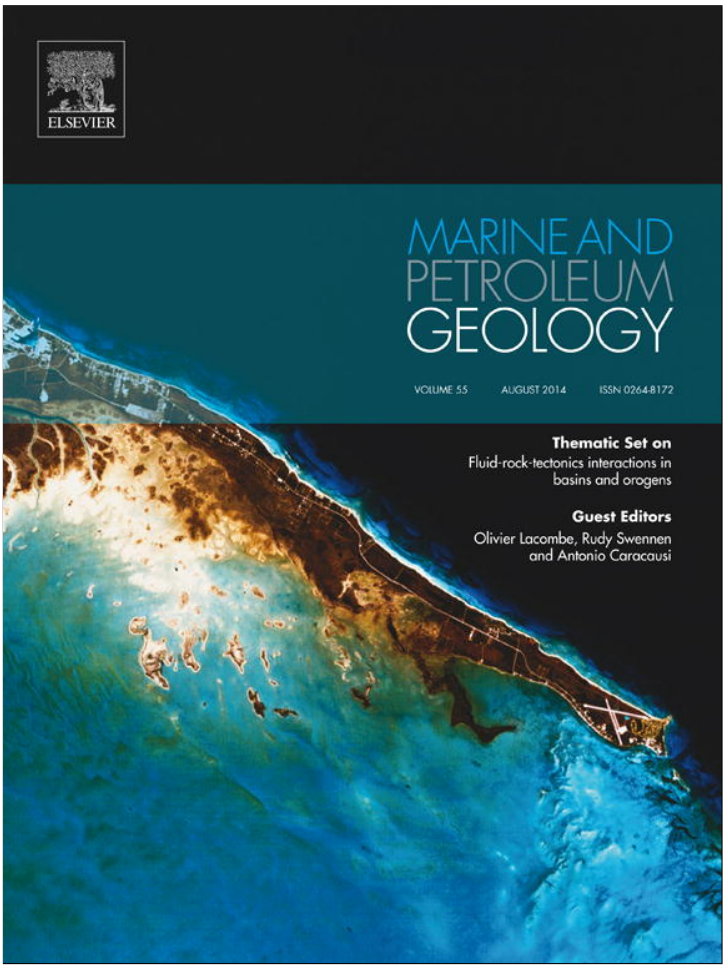

Marine and Petroleum Geology 55 (2014) 295–308

Contents lists available at ScienceDirect

Marine and Petroleum Geology

journal homepage: www.elsevier.com/locate/marpetgeo

A geochemical traverse along the "Sperchios Basin – Evoikos Gulf" graben (Central Greece): Origin and evolution of the emitted fluids

W. D'Alessandro [a,*], L. Brusca [a], K. Kyriakopoulos [b], S. Bellomo [a], S. Calabrese [c]

[a] Istituto Nazionale di Geofisica e Vulcanologia – Sezione di Palermo, Via U. La Malfa 153, 90146 Palermo, Italy
[b] National and Kapodistrian University of Athens, Dept. of Geology and Geoenvironment, Panepistimioupolis, 157 84 Ano Ilissia, Greece
[c] University of Palermo, Dept. DiSTeM, via Archirafi 36, 90123 Palermo, Italy

ARTICLE INFO

Article history:
Received 2 September 2013
Received in revised form
12 December 2013
Accepted 19 December 2013
Available online 29 December 2013

Keywords:
Greece
Rift zone
Geothermal activity
Helium isotopes
Carbon isotopes

ABSTRACT

The studied area is a 130 km long fast spreading graben in Central Greece. Its complex geodynamical setting includes both the presence of a subduction slab at depth responsible for the recent (Quaternary) volcanic activity in the area and the western termination of a tectonic lineament of regional importance (the North-Anatolian fault). A high geothermal gradient is made evident by the presence of many thermal springs with temperatures from 19 to 82 °C, that discharge along the normal faults bordering the graben.

In the period 2004–2012, 58 gas and 69 water samples were collected and their chemical and isotopic analysis revealed a wide range of compositions.

Two main groups of thermal waters can be distinguished on the basis of their chemical composition. The first, represented by dilute waters (E.C. <0.6 mS/cm) of the westernmost sites, is characterised by the presence of CH_4-rich and mixed N_2–CH_4 gases. The second displays higher salinities (E.C. from 12 to 56 mS/cm) due to mixing with a modified marine component. Reservoir temperatures of 150–160 °C were estimated with cationic geothermometers at the easternmost sites.

Along the graben, from west to east, the gas composition changes from CH_4- to CO_2-dominated through mixed N_2–CH_4 and N_2–CO_2 compositions, while at the same time the He isotopic composition goes from typical crustal values (<0.1 R/R_A) up to 0.87 R/R_A, showing in the easternmost sites a small (3–11%) but significant mantle input. The $\delta^{13}C$ values of the CO_2-rich samples suggest a mixed origin (mantle and marine carbonates).

1. Introduction

The studied area, the Sperchios Basin – Evoikos Gulf Graben (Fig. 1), has a complex geological history. Its high geodynamic activity has long been recognised. In fact it was documented in the earliest historical documents as well as in the Greek mythology (Fytikas et al., 1999). The legends tell us, in fact, that the battle between the Greek gods and the Titans occurred in this area, at the foot of Mt. Orthrys. This battle has been interpreted as a memory of intense prehistoric volcanic and seismic activity (Fytikas et al., 1999).

This area has been renowned as having one of the highest geothermal gradients in Greece outside the South Aegean active volcanic arc (SAAVA) (Fytikas and Kolios, 1979). It is a 130 km long actively spreading graben in Central Greece bordered by active faults (1 cm/a – Makris et al., 2001). Its complex geodynamical setting includes the presence of both a thinned crust (20 km thickness below the central part of the northern Evoikos Basin) and a subduction slab responsible for the recent (Quaternary) volcanic activity in the area (Makris et al., 2001). Some studies (Fytikas et al., 1976; Bellon et al., 1979; Papoulia et al., 2006) have suggested that the volcanic products of this area represent the northward continuation of the SAAVA.

Another important geodynamic feature that belongs to the study area is the western termination of the North-Anatolian fault (NAF). This right-lateral transform tectonic lineament of regional importance runs approximately east-west for more than 1000 km along the majority of the Anatolian peninsula and the northern Aegean sea. Previous authors have assumed that the opening of the Sperchios Basin graben together with the Kremasta Fault System accommodates the transcurrent movements of the NAF on the east with those of the Cephalonia Transform Fault on the west as a "bridge of failure" (Kilias et al., 2008). The high geothermal gradient of the area is made evident by the presence of many thermal

* Corresponding author. Tel.: +39 091 6849409; fax: +39 091 6849449.
E-mail addresses: w.dalessandro@pa.ingv.it, walter.dalessandro@ingv.it (W. D'Alessandro).

0264-8172/$ – see front matter © 2014 Elsevier Ltd. All rights reserved.
http://dx.doi.org/10.1016/j.marpetgeo.2013.12.011

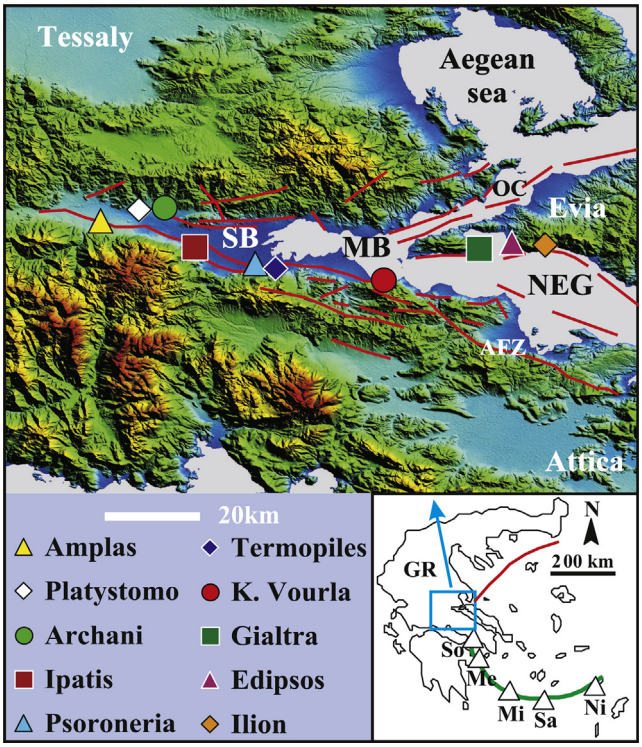

Figure 1. Elevation map of the study area. Main fault of the area are evidenced in red. The ten sampled thermal sites are shown with different symbols. The same symbols are used in all the figures. SB = Sperchios Basin; MB = Maliakos Bay; NEG = North Evia Gulf; AFZ = Atalanti fault zone; OC = Orei Channel. The inset shows the study area within the Hellenic territory: The green line shows the South Aegean Active Volcanic Arc (SAAVA) and the relative main active (Ni = Nisyros; Sa = Santorini; Mi = Milos; Me = Methana) or extinct (So = Sousaki) volcanic systems. The North Anatolian Fault (NAF) is shown in red. (For interpretation of the references to colour in this figure legend, the reader is referred to the web version of this article.)

springs with temperatures from 24 to 82 °C, that discharge along the normal faults bordering the graben.

The seismic activity of the area has been widely documented throughout history (Makris et al., 2001; Burton et al., 2004). The strongest earthquakes in the past were recorded in 426 BC, 1740 and 1894 (Papazachos and Papazachos, 1997) and were mostly associated with the Atalanti fault zone.

Pertessis (1961), Margomenou-Leonidopoulou (1976) and Antonopoulos (1992) believe that the significant variations of the thermal features of the area are correlated to important seismic events. The former refers to the description that Thucydides gave of the big earthquake of 426 BC that was responsible of a tsunami within the Maliakos Gulf. The historian states that the springs of Thermopiles and Edipsos dried up for three days, and when they had started to flow again at Edipsos they had changed their position. Pertessis (1961) recounts that the Gialtra spring's water became turbid; while Margomenou-Leonidopoulou (1976) refers that many new springs appeared in the area of Edipsos as a consequence of the earthquake of Atalanti in 1894.

Because it is inert along with all of the other noble gases, helium is an excellent natural tracer for fluid migration and can be extremely helpful in unravelling complex chemical processes that affect other more reactive species (e.g. Ballentine et al., 2002). Distinct mantle, crustal, and atmospheric sources are characterized by unique noble gas isotopic compositions, so their sources can be identified and used to constrain the fluid's history. Helium isotopes can also provide unequivocal evidence for the presence of mantle-derived volatiles.

Continental crust with negligible additions of mantle volatiles has low $^3He/^4He$ ratios of 0.02–0.1 R_A, reflecting a strong radiogenic ^4He component with a very low $^3He/^4He$ production ratio in the crust. The upper asthenosphere, as constrained by samples of mid-ocean ridge basalt (MORB), has a $^3He/^4He$ ratio of 8 ± 1 R_A that indicates the presence of primordial ^3He acquired during the Earth's formation (Ballentine et al., 2002). The European Sub-Continental lithospheric mantle (SCLM) has a $^3He/^4He$ ratio of 6.3 R_A (Gautheron et al., 2005). $^3He/^4He$ values between 0.1 and the appropriate mantle end-member (i.e., 6.3 or 8 R_A) are generally interpreted as a mixture of mantle and crustal sources. Lowering of the mantle value occurs through mixing with radiogenic ^4He as fluids move through the crust (Ballentine and Burnard, 2002). Conventionally, any air-corrected $^3He/^4He$ ratio $R_C/R_A > 0.1$ is considered to have an unequivocal mantle component (Ballentine et al., 2002) reflecting recent transport from the mantle. The presence of a significant mantle signature of He has often been used to track the input of mantle fluids in the crust either through the injection of magma batches (Sano and Wakita, 1985; Allard et al., 1997) or along deep-rooted regional transform faults. Examples of the latter mechanism can be found along the NAF in Turkey (Gülec et al., 2002), the San Andreas Fault in California (Kulongoski et al., 2013), the Dead Sea Trasform Fault (Torfstein et al., 2013) and the Karakoram Fault (Klemperer et al., 2013).

The studied area's thermal springs have been the subject of scientific investigations since the Pertessis's studies in the thirties (1937). Very few studies have been devoted to the geochemistry of the gases and those that have were limited to the most important manifestations (Barnes et al., 1986; Minissale et al., 1989; Shimizu et al., 2005). The geochemistry of the discharged waters has been studied more extensively and at least one chemical analysis, generally limited to the major ion composition, has been published for all of the thermal manifestations (Pertessis, 1961; Margomenou-Leonidopoulou, 1976; Garagunis, 1978; Minissale et al., 1989; Gartzos and Stamatis, 1996; Lambrakis and Kallergis, 2005; Duriez et al., 2008; Kelepertsis et al., 2009; Metaxas et al., 2010: Lambrakis et al., 2013).

As highlighted by the previous studies, fluids discharged in this area show a wide range of compositions. This is to be expected considering its complex geodynamic situation. However, despite the long list of previous studies, no comprehensive study of the geochemistry of the gases and the waters of the thermal features of the whole area has been undertaken up until now. In the period 2004–2012, 58 gas (either free or dissolved) and 69 water samples from the thermal manifestations were collected and analysed for their chemical and isotopic compositions. Eleven additional cold-water samples were collected to get insight in the chemical and isotopic composition of local groundwater. The present study contributes new data regarding the sampled manifestations since some measured parameters have never been determined for many sites. Considering that the area is a highly seismic zone, the present data, together with that of the previous authors, could be the necessary basis to study variations induced by the earthquakes of the region.

2. Study area and methods

2.1. Geology of the area

The Sperchios Basin and the Northern Evoikos Gulf form an active spreading graben with an extensional rate of about 1 cm/a, bordered on both sides by a series of extensive fault systems. Together with the nearby Corinthiakos Gulf graben, of parallel orientation and similar Quaternary age, it accommodates a large part of the SW–NE extension of central Greece (Roberts and Jackson, 1991).

The study area is built up from west to east by the terrains of (a) the Pindos zone, (b) the Parnassos–Ghiona zone, and (c) the Subpelagonian zone (Bornovas and Rondogianni-Tsiambaou, 1983). The latter covers most of the studied area, while the Pindos zone is only found in its easternmost part and the Parnassos–Ghiona zone only outcrops on the southern flank of the graben between the other two zones. The Pindos zone mainly consists of Paleocene pelitic and psammitic flysch, which is characterized by the presence of abundant organic material, as well as limestones and radiolarites of Jurassic to Cretaceous age. The Parnassos–Ghiona zone in the southernmost part consists of Paleocene flysch as well as limestone and dolomite of Triassic to Lower Jurassic age. The Subpelagonian zone consists of Cretaceous flysch, Mesozoic limestone of Upper Cretaceous and Upper Jurassic age, as well as shale and cherts. Ophiolitic thrust sheets cover a significant part of the zone. They consist of basic and ultrabasic igneous rocks, such as diabases, peridotites, pyroxenites, gabbros, serpentinites, laves, and tuffs. The peridotites are usually serpentinized. The lower part of the Sperchios Valley is covered by unconsolidated sediments of Pleistocene–Holocene age.

Furthermore, various small volcanic centres occur in the studied area. Radiometric dating obtained by several authors has shown that the volcanism of the central-east Greek mainland and North Euboea is of Miocene to Holocene age. Most of the volcanic centres show evidence of activity during Pliocene and Quaternary (Fytikas et al., 1976; Bellon et al., 1979; Papadopoulos, 1982, 1989; Pe-Piper and Piper, 1989, 2002).

In earlier studies (e.g. Fytikas et al., 1976; Bellon et al., 1979), it has been suggested that the Plio-Quaternary volcanism on the central-east Greek mainland and the island of Evia belongs to the inner part of the South Aegean volcanic arc. The associated seismicity occurring at intermediate depths of around 150 km results from the subduction of the Ionian oceanic lithosphere below the Hellenic arc. The origin of this volcanism was disputed by Papadopoulos (1982, 1989), because the volcanism in central-east Greece has different geophysical and geochemical features from that of the South Aegean Sea. In fact, in the South Aegean volcanic arc the geochemical characteristic of the lava is typically calc-alkaline. On the central-east Greek mainland, the chemistry of the lava ranges from calc-alkaline, to weak calc-alkaline, to weak alkaline. The argument is still under debate. Recently Papoulia et al. (2006) presented new geophysical data supporting the hypothesis that the volcanic activity of the area is connected to the present day volcanic arc while Innocenti et al. (2010) published new petrological data against it.

2.2. Sampling and analytical methods

Free bubbling gas samples were collected with an inverted funnel and stored in Pyrex bottles with two vacuum stopcocks. Samples for dissolved gas analyses were collected in glass vials sealed underwater.

All samples were analysed by gas chromatography using Carboxen 1000 columns, two detectors (HWD and FID) and argon as the carrier gas. The measurement precision was better than ±10%. Dissolved gases were determined using the analytical method proposed by Liotta and Martelli (2012), which is based on the equilibrium partition of gases between a liquid and a gas phase after introducing a known amount of carrier gas into the sampling vial.

The He-isotope ratio in free gas samples was analysed directly from the sample bottles after purification in the high-vacuum inlet line of the mass spectrometer. The isotope composition of dissolved He was analysed by headspace equilibration, following the method proposed by Inguaggiato and Rizzo (2004). He and Ne were then cryogenically separated and admitted into mass spectrometers. The $^{3}He/^{4}He$ ratio and ^{20}Ne content were analysed by a GVI Helix SFT mass spectrometer. Helium isotope compositions are given as R/R_A, namely $^{3}He/^{4}He$ of the sample versus the atmospheric $^{3}He/^{4}He$ ($R_A = 1.386 \times 10^{-6}$). Measured values were corrected for the atmospheric contamination of the sample (R_C/R_A) on the basis of its $^{4}He/^{20}Ne$ ratio (Sano and Wakita, 1985).

Carbon isotopes of CO_2 were analysed with a mass spectrometer (Finnigan MAT Delta S) after purifying the CO_2 under vacuum. $\delta^{13}C$ values of total dissolved inorganic carbon (TDIC) were determined by acid extraction following the method proposed by Capasso et al. (2005). $^{13}C/^{12}C$ ratios are reported here as $\delta^{13}C$ values (±0.1‰) with respect to the V-PDB standard. The isotopic composition of CH_4–C was measured using a Thermo TRACE GC and a Thermo GC/C III interfaced to a Delta Plus XP gas source mass spectrometer (±0.2‰ vs. V-PDB). The isotopic composition of N_2 was measured using a GV Instruments ARGUS mass spectrometer ($\delta^{15}N \pm 0.15$‰ vs. Air).

Hydrogen Sulfide concentrations were estimated in the field with Dräger tubes.

During the period Dec. 2004–Nov. 2012, 80 water samples were collected in the area (Table 1). Sixty-nine samples were taken from the thermal springs and eleven from the cold aquifers.

The water temperature, pH, Eh and electric conductivity were measured in the field with portable instruments. Total alkalinity was determined by titration with 0.1 M HCl on unfiltered samples. Major anions (F^-, Cl^-, NO_3^- and SO_4^{2-}) were determined by ionic chromatography on filtered samples while major cations (Na^+, K^+, Mg^{2+} and Ca^{2+}) were determined by ionic chromatography on filtered and acidified (0.2% HNO_3) samples.

For trace element analysis, water samples were filtered with 0.45 μm Millipore MF filters and stored in 50 ml PP (polypropylene) bottles, and acidified to a pH of ~2 with ultrapure concentrated HNO_3. Some trace elements (Li, B, Mn, Fe, As, Rb, Sr and Ba) were analysed by inductively coupled plasma mass spectrometry (ICP-MS) using an Agilent 7500ce instrument. Calibration solutions for all of the investigated elements were prepared daily using an appropriate dilution of 100 mg l^{-1} and 1000 mg l^{-1} of stock standard solutions (Merck) with 0.14 mol l^{-1} high-purity nitric acid. The accuracy of the method was checked analysing certified reference materials of natural waters (Nist 1643e, Environment Canada TM-24.3 and TM-61.2, Spectrapure Standards SW1 and SW2) at regular intervals during sample analysis. The experimental concentrations determined in this study were in accordance with these certified values (within ±5%). Matrix induced signal suppressions and instrumental drift were corrected by internal standardization. Indium was used for elements up to a mass of 138 (^{138}Ba), and rhenium was used for heavier elements.

Silica content was determined with ICP-OES (Yobin Ultima) as well as B, Mn and Fe in saline waters.

Oxygen and hydrogen isotopic compositions of the water were determined by mass-spectrometry on unfiltered samples and expressed in ‰ with respect to the international standard V-SMOW (Vienna Standard Mean Ocean Water). The uncertainties are ±0.1‰ for $\delta^{18}O$ and ±1‰ for δD (±1 σ).

All chemical and isotopic analyses of the gas and water samples were carried out at the laboratories of the INGV-Palermo.

3. Results and discussion

3.1. Geochemistry of the waters

The sampled thermal manifestations display a rather large range both for their physical–chemical parameters and their water composition (Table 1). They can be roughly subdivided into low-salinity waters (TDS < 0.5 g/l; Amplas, Platystomo and Archani) and high-salinity waters with a Sodium-Chloride composition (TDS 9 – 35 g/l; the remaining manifestations) (Fig. 2). With the

Table 1
Chemical and isotopic composition of the waters sampled in the study area.

	Sample	Date	T °C	pH	Cond µS/cm	Na mg/l	K mg/l	Mg mg/l	Ca mg/l	F mg/l	Cl mg/l	NO_3 mg/l	SO_4 mg/l	Alk mg/l	SiO_2 mg/l	Li µg/l	B µg/l	Mn µg/l	Fe µg/l	As µg/l	Rb µg/l	Sr µg/l	Ba µg/l	$\partial^{18}O$ ‰	∂D ‰
Amplas	Amplas pond	6-02-2005	18.9[a]	9.51	445	88.7	1.17	2.31	13.6	3.80	34.0	0.62	32.2	189	72.1	5.43	5540	42.5	39.1	4.81	2.06	77.6	8.95	−9.80	−63.5
	Amplas pond	28-03-2008	19.5[a]	8.30	343	77.7	1.56	1.34	8.6	4.01	28.0	0.62	23.0	153	54.8	7.24	6380	51.7	72.1	0.28	2.54	53.2	6.46	−8.55	−54.2
	Amplas pond	12-10-2008	18.5[a]	8.70	433	90.1	2.27	2.97	20.1	3.44	30.6	15.1	48.5	183	50.1	10.7	6760	355	73.6	2.00	3.08	161	12.4	−8.78	−58.7
	Amplas well	26-06-2009	24.0	9.72	383	93.1	0.78	0.36	1.6	4.56	34.7	0.00	25.4	171	59.9	8.36	8300	n.d.	1.29	0.20	2.02	30.7	4.13	−9.90	−63.0
Platystomo	Platystomo	6-02-2005	26.0	7.33	436	23.9	0.39	17.7	51.5	0.19	16.0	0.00	4.80	281	48.8	5.94	314	6.96	18.4	21.4	0.72	332	10.8	−8.50	−53.0
	Platystomo	28-03-2008	26.3	7.37	434	24.6	0.78	17.5	49.7	0.23	19.9	0.00	12.5	256	43.3	8.67	400	6.28	1.48	n.d.	0.75	329	8.53	−8.48	−53.7
	Platystomo	26-06-2009	25.1	7.41	400	29.2	0.39	16.8	40.3	0.38	20.2	0.00	17.3	241	42.1	9.18	643	7.29	0.95	<0.1	0.78	379	10.6	−8.30	−52.0
	Platystomo 2	28-03-2008	23.7	7.44	392	28.0	0.78	17.1	40.7	0.29	17.7	0.00	8.16	244	46.0	9.42	506	7.21	5.49	n.d.	0.74	358	8.00	−8.40	−53.8
Archani	Archani	28-03-2008	27.5	11.2	570	22.8	0.78	0.12	35.9	0.02	14.5	0.00	0.48	146	5.8	0.32	52.6	n.d.	0.96	n.d.	0.63	50.5	3.68	−8.55	−60.4
	Archani	26-06-2009	27.6	11.3	538	23.2	0.78	0.12	35.7	n.d.	17.4	0.00	0.96	153	5.3	0.29	69.0	n.d.	0.19	<0.1	0.63	52.7	6.41	−8.92	−58.0
Ipatis	Ipatis	6-02-2005	29.8	6.36	13,860	1990	172	259	934	n.d.	4200	0.00	47.0	2540	37.9	4310	6360	14.6	292	259	566	26,900	1650	−7.50	−53.0
	Ipatis	14-09-2006	30.5	6.40	12,400	2020	171	275	771	1.50	4300	0.00	52.8	1940	31.3	4160	6160	24.1	495	5.78	727	30,800	1940	−7.36	−53.0
	Ipatis	28-03-2008	30.0	6.05	14,450	2010	172	297	971	1.43	4230	0.00	46.6	2510	37.7	3470	5530	18.0	365	5.42	627	27,600	1870	−7.66	−52.2
	Ipatis	11-10-2008	30.3	6.38	14,410	2040	176	285	1030	0.87	4350	0.00	50.4	2630	27.5	3980	6130	17.6	105	2.61	616	28,800	1810	−7.67	−53.7
	Ipatis	26-06-2009	31.0	6.34	12,720	2270	188	313	780	n.d.	4680	0.00	129	2550	29.8	4010	5910	19.5	82.6	5.46	645	28,900	1900	−7.67	−49.0
	Loutra Ipatis	11-10-2008	32.3	6.33	13,460	1990	176	285	486	0.87	4240	0.00	57.3	1050	29.4	3920	6020	31.3	50.7	4.70	592	28,000	1850	−7.90	−54.0
Psoroneria	Psoroneria 1	12-12-2004	32.5	6.18	34,300	8700	273	690	1190	n.d.	16,100	0.00	1910	933	18.9	n.d.	n.d.	n.d.	n.d.	n.d.	n.d.	n.d.	n.d.	−1.16	−11.0
	Psoroneria 1	27-03-2008	32.3	6.04	34,000	6810	246	500	888	2.36	11,900	0.00	1350	799	20.4	471	2980	135	976	15.9	188	9970	88.5	−3.03	−20.4
	Psoroneria 2	12-12-2004	33.2	6.30	29,200	4090	140	363	669	n.d.	7720	45.9	965	689	19.0	n.d.	n.d.	n.d.	n.d.	n.d.	n.d.	n.d.	n.d.	−4.99	−33.0
	Psoroneria 2	14-09-2006	31.0	6.30	17,300	4450	152	386	728	1.75	8010	18.4	1010	671	21.4	382	2260	44.0	322	4.61	143	7380	94.6	−5.22	−35.0
	Psoroneria 2	12-02-2008	31.6	6.71	20,600	4130	147	397	697	1.54	7590	12.7	869	705	23.4	457	2710	55.9	283	9.38	155	8270	98.6	−4.85	−25.8
	Psoroneria 2	27-03-2008	34.7	6.10	33,000	6860	239	498	914	2.19	12,300	0.00	1440	802	23.3	478	3060	99.5	733	11.2	188	9800	90.2	−2.96	−21.2
	Psoroneria 2	28-06-2009	33.4	6.13	26,000	5700	187	479	828	n.d.	7370	1.12	912	659	27.2	449	2720	76.9	470	12.0	167	9080	90.4	−5.30	−30.0
	Psoroneria	7-11-2012	33.3	6.22	25,000	3730	137	307	584	3.04	6770	0.00	875	720	n.d.	n.d.	n.d.	n.d.	n.d.	n.d.	n.d.	n.d.	n.d.	n.d.	n.d.
Thermopiles	Thermopiles	2-12-2004	40.3	6.01	14,000	2390	104	208	596	3.61	4540	0.00	419	979	34.1	n.d.	n.d.	n.d.	n.d.	n.d.	n.d.	n.d.	n.d.	−6.74	−40.0
	Thermopiles	10-02-2005	40.0	6.06	14,430	2500	111	204	545	1.69	4690	12.6	454	1000	41.5	1320	3980	1.30	42.3	211	216	11,400	102	−6.96	−42.0
	Thermopiles	10-11-2005	40.2	6.36	14,690	2580	114	208	585	3.00	4850	0.00	439	967	36.7	n.d.	n.d.	n.d.	n.d.	n.d.	n.d.	n.d.	n.d.	−6.69	−41.0
	Thermopiles	14-09-2006	40.5	6.12	n.m.	2740	120	230	647	2.74	5170	0.00	478	1010	36.1	1440	4300	3.11	18.8	84.8	278	13,200	128	−6.70	−42.0
	Thermopiles	12-02-2008	41.2	6.59	13,600	2670	123	226	603	4.15	4990	0.00	441	991	38.7	1490	4280	1.56	20.8	302	275	13,300	123	−6.60	−36.8
	Thermopiles	28-03-2008	41.1	6.06	18,200	2640	121	221	573	2.36	5080	0.00	447	946	38.1	1250	3990	1.72	17.6	72.1	258	12,500	123	−6.38	−40.5
	Thermopiles	28-06-2008	41.0	6.90	15,230	2710	124	224	585	1.64	5410	0.00	448	976	39.5	1470	4400	2.01	34.1	340	252	13,400	116	−6.64	−41.2
	Thermopiles	12-10-2008	40.8	6.13	18,400	2680	122	224	577	1.88	5190	0.00	480	915	29.2	1360	5670	24.5	29.3	331	237	13,100	114	−6.49	−42.1
	Thermopiles	28-06-2009	41.6	6.03	13,460	2530	114	213	559	1.52	4610	0.00	443	946	35.8	1280	3790	2.39	53.6	134	241	12,200	113	−6.86	−39.0
	Thermopiles	17-06-2011	39.0	6.10	n.m.	1630	73	131	430	1.22	3050	0.00	310	830	22.4	794	2340	3.07	97.6	325	192	8670	100	−7.15	−44.0
	Thermopiles	7-11-2012	40.0	6.05	11,600	2240	104	171	524	2.28	4170	0.00	400	872	n.d.	n.d.	n.d.	n.d.	n.d.	n.d.	n.d.	n.d.	n.d.	n.d.	n.d.
Kammena Vourla	Kammena Vourla	2-12-2004	35.3	6.25	21,200	4040	133	299	721	n.d.	7510	0.00	734	644	51.1	544	2510	875	1790	n.d.	n.d.	5930	129	−5.12	−28.0
	Kammena Vourla	10-11-2005	35.1	6.66	19,420	3780	130	265	685	n.d.	6830	0.00	676	726	51.2	n.d.	n.d.	n.d.	n.d.	n.d.	n.d.	n.d.	n.d.	−5.44	−33.0
	Kammena Vourla	14-09-2006	39.3	6.23	18,400	5090	169	359	864	2.09	8980	0.00	1020	921	47.5	685	5780	1190	2470	64.0	138	7640	137	−4.93	−30.0
	Kammena Vourla	12-02-2008	37.8	6.71	18,500	3790	136	264	614	1.59	7210	0.00	689	698	46.0	608	5090	961	2020	55.3	111	6100	115	−5.22	−28.2
	Kammena Vourla	27-03-2008	37.9	6.19	23,300	4080	147	274	642	2.19	7510	0.00	705	671	45.5	502	4790	925	1490	50.1	104	5630	106	−5.01	−31.8
	Kammena Vourla	12-10-2008	39.1	6.30	27,300	4540	161	329	787	1.22	8550	0.00	828	671	24.3	565	6350	1090	2320	76.5	108	6690	111	−4.82	−30.3
	Kammena Vourla	7-11-2012	36.8	6.26	20,000	4460	158	287	701	3.61	8090	0.00	786	702	n.d.	n.d.	n.d.	n.d.	n.d.	n.d.	n.d.	n.d.	n.d.	n.d.	n.d.
	Kammena Vourla 2	2-12-2004	41.3	6.10	24,600	4710	159	320	833	n.d.	8730	0.00	856	711	36.4	629	3960	548	2640	74.7	n.d.	6580	97.9	−4.55	−26.0
	Kammena Vourla 3	2-12-2004	38.6	6.13	23,000	4440	147	303	794	3.12	8310	0.00	810	708	32.5	n.d.	n.d.	n.d.	n.d.	n.d.	n.d.	n.d.	n.d.	−4.67	−27.0
	Kammena Vourla 4	10-02-2005	40.5	6.18	23,500	4970	172	327	809	n.d.	9050	0.00	899	1080	62.9	676	4140	115	55.8	34.3	n.d.	6780	83.8	−4.50	−28.0

Table 1 (*continued*)

	Sample	Date	T °C	pH	Cond µS/cm	Na mg/l	K mg/l	Mg mg/l	Ca mg/l	F mg/l	Cl mg/l	NO_3 mg/l	SO_4 mg/l	Alk mg/l	SiO_2 mg/l	Li µg/l	B µg/l	Mn µg/l	Fe µg/l	As µg/l	Rb µg/l	Sr µg/l	Ba µg/l	$\partial^{18}O$ ‰	∂D ‰
	Koniavitou 1	2-12-2004	32.4	6.22	16,000	2940	97.8	203	564	n.d.	5370	0.00	507	747	24.9	413	1710	5.32	n.d.	n.d.	n.d.	4150	69.5	−5.90	−34.0
	Koniavitou 1	26-06-2009	33.1	6.23	15,900	3290	107	210	597	n.d.	6270	0.00	600	647	25.3	511	3480	24.0	100	3.58	107	5120	97.5	−5.84	−32.0
	Koniavitou 2	2-12-2004	35.0	6.13	22,000	4040	136	263	775	n.d.	7590	0.00	702	702	31.8	n.d.	n.d.	n.d.	n.d.	n.d.	n.d.	n.d.	n.d.	−5.18	−30.0
	Kyriakou	2-12-2004	33.2	6.10	18,000	3340	110	232	654	n.d.	6300	0.00	597	692	25.0	496	2120	n.d.	83	7.97	n.d.	5020	72.7	−5.60	−31.0
Gialtra	Gialtra	15-09-2006	44.0	6.43	39,500	10,300	331	632	1690	n.d.	19,800	0.00	2550	275	23.4	647	4810	28.6	652	49.0	160	15,300	87.8	−0.27	−2.0
	Gialtra	29-03-2008	43.5	6.58	56,700	10,200	334	637	1640	1.63	19,100	0.00	2340	262	24.8	577	4630	26.1	555	45.1	147	14,300	83.8	0.04	−1.7
	Gialtra	27-06-2009	43.7	6.33	41,500	10,300	324	629	1640	n.d.	18,800	0.00	2430	271	19.4	658	5240	24.4	606	50.8	148	14800	93.5	0.27	−2.0
	Gialtra 2	29-03-2008	44.0	6.70	56,000	10,200	332	619	1630	1.90	18,900	0.00	2400	256	25.2	538	4310	24.9	368	38.9	140	13,500	79.8	0.00	−1.6
Edipsos	Damaria	12-12-2004	74.0	6.14	43,900	9850	332	316	1630	7.22	18,800	0.00	1090	595	57.9	n.d.	n.d.	n.d.	n.d.	n.d.	n.d.	n.d.	n.d.	0.25	−4.0
	Damaria	29-03-2008	72.0	6.00	56,000	9800	339	316	1620	5.23	18,500	0.00	1040	610	62.9	1150	8860	74.4	2750	31.0	229	14,700	279	−0.01	−4.3
	Damaria	27-06-2009	71.1	5.92	43,000	10,100	331	310	1560	n.d.	18,300	0.00	1090	650	53.0	1480	9880	76.2	3420	30.5	237	15,800	272	−0.35	−4.0
	Damaria	9-11-2005	65.4	6.02	46,500	10,400	353	330	1780	n.d.	19,400	0.00	1120	662	58.3	n.d.	n.d.	n.d.	n.d.	n.d.	n.d.	n.d.	n.d.	0.29	−2.0
	Damaria	9-11-2005	82.2	6.26	46,300	10,000	338	317	1700	n.d.	18,900	0.00	1100	662	56.2	n.d.	n.d.	n.d.	n.d.	n.d.	n.d.	n.d.	n.d.	0.08	−2.0
	Papaioannou	9-11-2005	52.2	6.31	44,200	9680	331	302	1480	n.d.	17,600	0.00	1030	482	65.8	n.d.	n.d.	n.d.	n.d.	n.d.	n.d.	n.d.	n.d.	−0.26	−6.0
	Platania	27-08-2009	66.0	6.70	38,000	10,500	335	338	1650	n.d.	19,700	0.00	1140	348	54.0	1560	12,500	70.8	832	82.1	248	13,300	328	n.d.	n.d.
	Sylla	9-11-2005	59.0	6.24	41,200	9140	310	301	1490	n.d.	16,400	0.00	1000	522	53.3	n.d.	n.d.	n.d.	n.d.	n.d.	n.d.	n.d.	n.d.	−0.90	−9.0
	Termopotamos	9-11-2005	82.1	6.30	46,200	10,200	344	325	1760	n.d.	18,900	0.00	1090	650	57.7	n.d.	n.d.	n.d.	n.d.	n.d.	n.d.	n.d.	n.d.	0.04	−3.0
	Termopotamos	15-09-2006	73.0	6.08	40,800	10,600	360	343	1800	5.26	20,200	0.00	1160	641	56.0	1570	10,200	49.0	1170	13.5	264	16,000	335	0.01	−5.0
	Edipsos 2	10-02-2005	80.0	6.35	44,000	9850	319	284	1610	4.37	17,900	0.00	1100	692	77.9	1650	10,900	63.6	913	563	221	15,100	282	−0.22	−3.0
Ilion	Ilion	10-02-2005	63.5	6.00	30,800	6060	181	203	1470	n.d.	11,900	0.00	751	674	136	3430	12,000	486	12,600	658	263	26,900	211	−3.59	−25.0
	Ilion	15-09-2006	64.0	6.13	28,800	6570	206	239	1550	3.61	12,700	0.00	802	644	115	3150	11,000	565	17,800	188	311	28,600	236	−3.51	−26.0
	Ilion	29-03-2008	63.0	6.00	46,000	6340	204	234	1530	4.20	12,600	0.00	711	573	127	2590	9870	530	14,600	176	280	26,700	227	−3.08	−24.3
	Ilion	27-06-2009	63.8	5.97	31,500	6510	192	247	1500	n.d.	12,200	0.00	802	644	117	3140	10,900	545	17,700	190	287	28,400	228	−3.60	−24.0
	Ilion	27-08-2009	63.0	6.28	27,200	6380	186	239	1580	5.32	12,500	0.00	747	671	111	3200	11,100	545	18,000	204	298	25,900	234	n.d.	n.d.
Cold	Cloni 1	6-02-2005	6.5	7.55	245	1.15	0.39	2.43	55.7	0.06	1.77	0.81	2.88	174	7.1	0.79	71.9	0.27	4.26	19.5	0.13	93.3	27.2	−9.85	−61.0
groundwaters	Cloni 2	6-02-2005	8.4	7.24	839	124	2.74	25.4	62.3	3.23	10.6	0.00	17.8	601	30.6	50.3	1550	46.7	12.6	19.2	1.83	702	323	−9.10	−59.0
	Cloni 3	6-02-2005	14.5	7.34	768	59.5	3.52	31.5	87.0	0.57	6.74	0.00	79.2	470	32.1	37.2	477	78.4	22.8	10.8	2.75	4750	177	−8.93	−55.0
	Bitoli	6-02-2005	7.9	7.50	429	41.2	0.78	18.2	36.9	1.12	11.7	0.00	7.68	287	44.3	6.74	1504	15.4	9.81	15.3	0.51	429	9.8	−9.00	−58.0
	Krio T.	9-11-2005	22.3	7.55	2220	281	11.3	40.7	156	n.d.	511	3.10	54.7	451	23.0	n.d.	n.d.	n.d.	n.d.	n.d.	n.d.	n.d.	n.d.	−8.74	−50.0
	Gialtra 1	29-03-2008	16.0	7.45	1130	87.4	31.7	38.8	117	0.15	115	192	72.0	360	34.4	7.80	339	n.d.	2.70	3.54	1.64	212	136	−8.00	−48.2
	Gialtra 2	29-03-2008	15.5	7.14	1139	86.7	28.9	44.2	116	0.17	114	208	71.0	360	33.6	8.78	386	0.09	2.86	4.99	1.27	229	138	−8.00	−48.9
	Achilea	11-10-2008	14.6	7.44	693	13.5	0.02	39.9	112	0.05	106	0.49	27.0	360	19.6	1.44	16.8	25.2	11.5	0.18	0.23	134	2.82	−9.06	−59.2
	Asproneri	29-06-2009	21.4	7.55	995	110	4.30	38.5	77.2	n.d.	200	0.00	28.8	346	14.7	14.3	108	0.02	3.10	5.31	3.77	262	27.1	−8.10	−49.0
	Pedopoli	27-08-2009	20.0	7.22	516	9.66	0.39	25.3	73.1	0.19	15.6	1.86	13.4	329	9.2	1.33	17.1	0.53	4.95	0.36	0.33	63.3	17.1	−9.30	−55.0
	Panagia Dinious	27-08-2009	14.0	7.13	682	22.1	0.78	29.6	99.0	0.19	33.3	3.10	20.2	427	20.4	3.39	16.1	0.52	2.15	1.71	0.34	106	71.6	−7.90	−46.0
	Ag. Eleni	27-08-2009	17.0	7.25	635	27.8	4.69	42.9	62.9	0.21	28.0	1.74	6.72	430	26.3	3.48	38.7	11.0	4.86	2.57	0.78	244	42.7	−7.20	−44.0

[a] temperature measurement unreliable because of the strong influence of the air temperature on the slow flowing water in the sampled pond. n.d. = not determined.

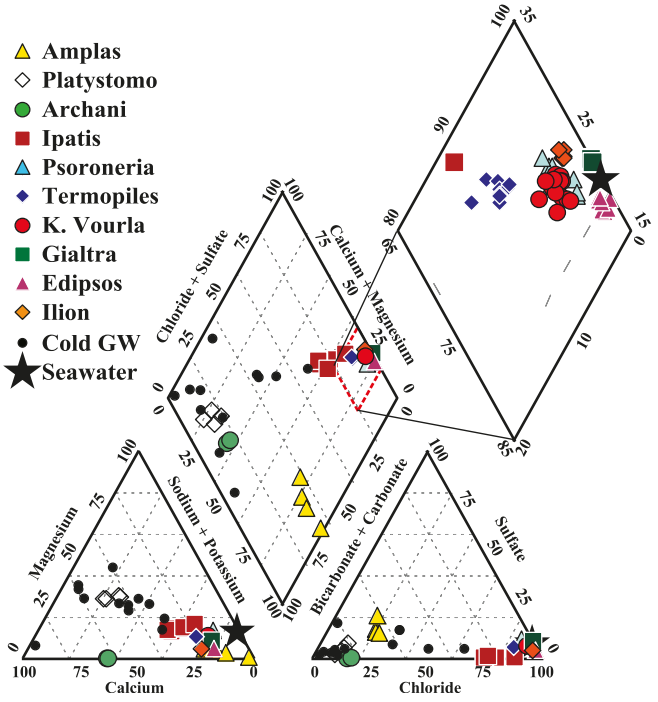

Figure 2. Piper diagram showing the composition of the major ions in the sampled waters. The composition of seawater is evidenced with the star symbol. The most saline waters are crowded close to seawater and are shown with only one point for each site. The rhomb on the right is an enlargement showing all the collected samples of the high-saline waters.

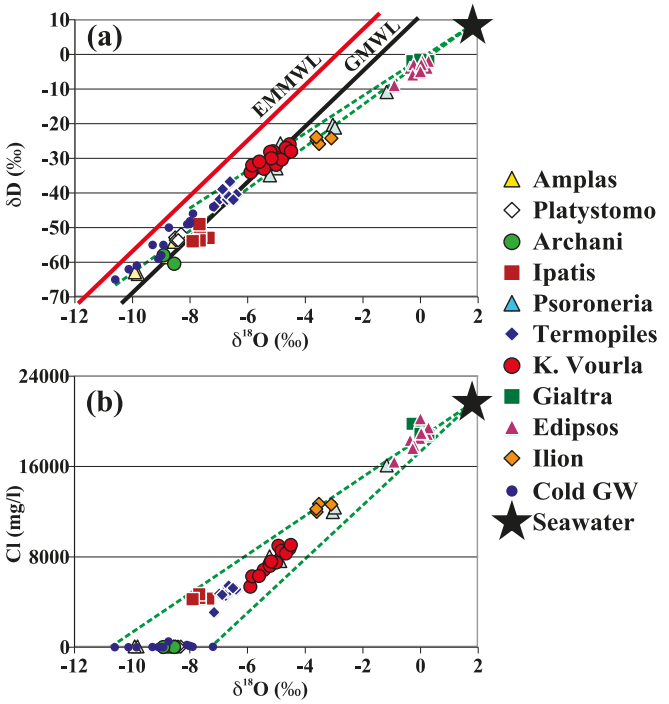

Figure 3. δD-δ^{18}O (a) and Cl-δ^{18}O (b) binary plots. The Global Meteoric Water Line (GMWL – Craig, 1961) and the Eastern Mediterranean Meteoric Water Line (EMMWL – Gat and Carmi, 1970) and Aegean Sea Water point are also shown. Mixing between Seawater and meteoric water is evidenced with green dashed lines. (For interpretation of the references to colour in this figure legend, the reader is referred to the web version of this article.)

exception of Amplas, which shows a Sodium-bicarbonate composition, the low salinity waters display water compositions that are very close to that of the Calcium-bicarbonate cold groundwater of the area (Fig. 2). In the δD-δ^{18}O diagram (Fig. 3a), the cold groundwater falls between the Global Meteoric Water Line (GMWL – Craig, 1961) and the Eastern Mediterranean Meteoric Water Line (EMMWL – Gat and Carmi, 1970), which is typical of the area's meteoric water recharge (Dotsika et al., 2010). The isotopic composition of this groundwater is compatible with the prevailing recharge along the nearby mountain ranges that reach altitudes of over 2000 m. In the δD-δ^{18}O and Cl-δ^{18}O graphs (Fig. 3), the high salinity water plot along the mixing line between the Aegean seawater and the average meteoric recharge of the area represented by the cold groundwater. In these graphs, no isotopic shift could be identified, excluding isotopic exchange with rocks in the hydrothermal aquifers. The low salinity waters collected at Amplas, Platystomo and Archani display isotope and chloride values falling in the same range as the local cold groundwater.

The seawater – meteoric water mixing trend can also be seen on the Na–Cl plot (Fig. 4a), further supporting the hypothesis of a contamination of the hydrothermal systems by the Aegean seawater. However, considering that chloride is a conservative element, other binary plots show significant modifications of the seawater-contaminated waters due to gas–water–rock interactions within the hydrothermal circuit. Alkalinity (Fig. 4b) is strongly enriched, likely due to the dissolution of the abundant CO_2-rich gas phase. Calcium (Fig. 4c), B (Fig. 4d), F, Li, Rb, Sr and Ba (not shown) are also enriched with respect to chloride. On the contrary, Mg and SO_4 are depleted (Fig. 4e–f), the former being incorporated in secondary minerals and second either reduced to H_2S or precipitated as anhydrite.

Although the chemical composition of the high-salinity waters can be entirely explained by a variable mixture of modified seawater with a meteoric water component, the composition of the low-salinity waters cannot be produced by these processes. Platystomo's waters show chemical features consistent with those of the cold groundwater of the area, indicating an evolution similar to that of local meteoric water. On the contrary, Amplas's waters have lower Ca and Mg contents, indicating a removal through carbonate phase deposition and very high B contents. Archani waters show very high pH values, low sulphate content and very low Mg concentrations, which is typical of waters that circulate deeply in ophiolithic rocks (Cipolli et al., 2004). On the contrary, Mg enrichment of cold groundwater is typical of the first weathering stages of ophiolithic rocks (Cipolli et al., 2004) while excess SO_4 could be inherited from the meteoric recharge which generally has much higher SO_4/Cl ratios than seawater due to anthropogenic derived S compounds (D'Alessandro et al., 2013).

As shown by the triangular graph of Giggenbach (Fig. 5), most of the waters are immature and therefore unsuitable for geothermometric estimations. Only those from the easternmost sites (Gialtra, Ilion and Edipsos) demonstrate having attained a partial chemical equilibrium at a temperature range of 150–170 °C. Silica geothermometers (quartz – Fournier, 1977) only give similar estimations (142–154 °C) for Ilion, while estimated values for Gialtra (61–71 °C) are strongly influenced by shallow mixing processes. Precipitation of colloidal silica probably lowers the estimated temperatures at Edipsos (104–123 °C). The emerging waters have, in fact, a milky appearance due to the precipitating phases.

3.2. Geochemistry of the gases

The gas samples display a very large variability in chemical composition (Table 2). They show CH_4-dominated (Amplas), CO_2-dominated (Ipatis, Thermopiles, Edipsos and Ilion), N_2-dominated (Platystomo, Archani and Gialtra) or mixed N_2–CO_2 (Psoroneria and Kamena Vourla) compositions. Methane diminishes rapidly, going from west to east from about 900,000 μmol/mol at Amplas to

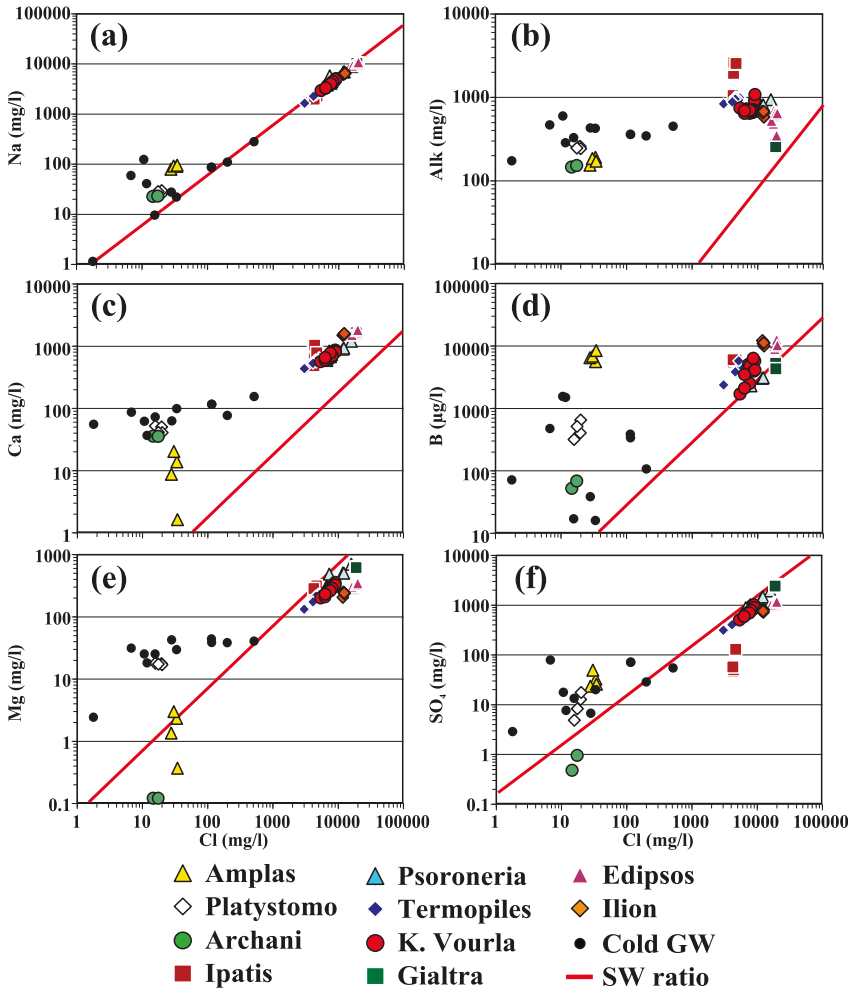

Figure 4. Ion-Chloride binary plots. The plotted ions are respectively Sodium (a), Alkalinity (b), Calcium (c), Boron (d), Magnesium (e) and Sulphate (f). The red line represents the respective Ion-Chloride ratio in seawater. (For interpretation of the references to colour in this figure legend, the reader is referred to the web version of this article.)

about 1000 μmol/mol in all of the sites east of Psoroneria (Fig. 6). Helium ranges from 0.3 up to 1140 μmol/mol and shows a fairly positive correlation with N_2 (Fig. 7). The He/N_2 ratios are of orders of magnitudes higher than those of the atmospheric ones, indicating enrichment in crustal or/and mantle He. On the contrary, N_2/Ar ratios generally fall between the values of the atmosphere and that of air-saturated water. Assuming that the N_2 is completely derived from the atmosphere through meteoric recharge, the expected N_2/Ar ratio for these gases should coincide with that of ASW. The slight difference between the measured N_2/Ar ratios and that of ASW suggest an additional source. A few measured $\delta^{15}N(N_2)$ values ranging from 0.5 to 2.5‰ argue in favour of a crustal source. Only a few samples have detectable H_2 (>2 μmol/mol) concentrations with values that are always lower than 50 μmol/mol.

The very low dissolved CO_2 concentrations in the samples from Archani (measured pCO_2 values of $2–3 \times 10^{-5}$ atm, lower than the atmospheric value of 4×10^{-4} atm), are typical of hyperalkaline waters derived from ophiolythic aquifers (Etiope et al., 2011). The low temperature serpentinisation process of the ultrabasic rocks within such aquifers results in very reducing conditions and the consequently high H_2 concentrations favour the reduction of CO_2 to CH_4 (Etiope et al., 2011).

The $O_2–N_2–CO_2$ triangular plot (Fig. 8) reveals N_2/O_2 ratios that are generally much higher than those in the atmosphere. This indicates that the atmospheric component, derived from meteoric recharge, has been modified by organic and inorganic redox reactions in the subsoil and possibly also by the addition of crustal N_2. No sample plots close to the point representing atmospheric air, thus the possibility of strong air contamination during sampling can be excluded.

3.3. Helium isotopes

Helium isotopic values in the study area vary from 0.02 to 0.85 R_C/R_A (Table 2). The few published data available (Shimizu et al., 2005; University of Cambridge He database, 1994 in Pik and Marty, 2009) agree with our data.

Assuming that the helium in the gas samples is composed of three components, we can calculate their relative contribution using the following equations:

$$(^3He/^4He) = (^3He/^4He)_M \times M + (^3He/^4He)_C \times C + (^3He/^4He)_A \times A$$

$$1/(^4He/^{20}Ne) = M/(^4He/^{20}Ne)_M + C/(^4He/^{20}Ne)_C + A/(^4He/^{20}Ne)_A$$

$$M + C + A = 1$$

where M, C and A represent the fraction of mantle, continental crust and atmospheric helium (^4He) contribution, respectively, and the

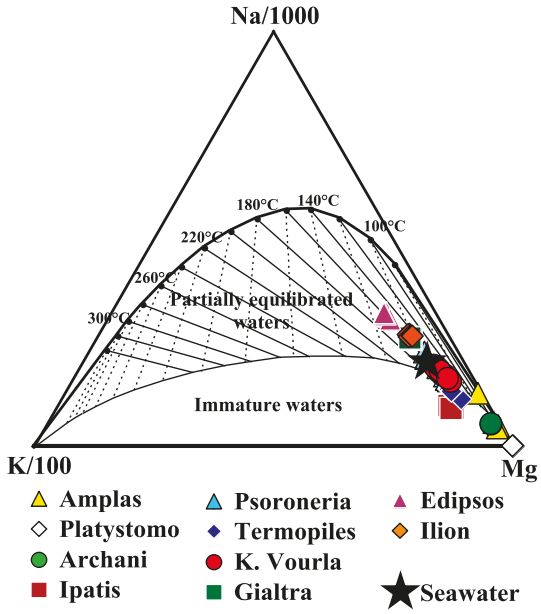

Figure 5. Na–K–Mg ternary diagram. The diagram provides at-a-glance information on the degree of water–rock equilibrium for low-temperature geothermal systems (Giggenbach and Corrales, 1992). Although most of the sampled waters fall close to the Mg vertex, the plot allows for a clear distinction of the partially equilibrated thermal waters and the immature cold waters into well separated groups. Bold line indicates the full equilibrium line; the thin line indicates the boundary between immature and partially equilibrated waters.

subscripts *m*, *c* and *a* denote mantle, continental crust and atmospheric values, respectively. The end-members used in the present calculation were:

$$(^3He/^4He)_M = 6.3\,R_A;\ (^4He/^{20}Ne)_M = 1000;$$

$$(^3He/^4He)_C = 0.02\,R_A;\ (^4He/^{20}Ne)_C = 1000;$$

$$(^3He/^4He)_A = 1\,R_A;\ (^4He/^{20}Ne)_A = 0.318.$$

Instead of the generally used MORB-type mantle, we used a SCLM-type mantle as our end-member. There is a great deal of evidence supporting such an end-member in the European and Mediterranean area (Dunai and Baur, 1995; Gautheron et al., 2005; Torfstein et al., 2013). The end-member value used in the calculations (6.3 R_A) is that estimated for the European SCLM by Gautheron et al. (2005), which is almost the same as that estimated by Shimizu et al. (2005) for the Aegean region based on the highest values measured in gas manifestations (6.2 R_A).

The relative contributions of the three components found in the present study are shown in Table 2. Air contamination is generally very limited and most of the samples display He/Ne values higher than 10 (Fig. 9). This is reflected in the atmospheric contributions, which are lower than about 3% and mostly below 1% (Table 2). Only three samples have He/Ne values around 2.5, and these needed to be corrected significantly due to atmospheric contributions between 11 and 14%. The sample taken at Archani displays a He/Ne value as low as 0.76, indicating a high atmospheric contamination (~37%). Although the resulting R_C/R_A value (0.02) is affected by high incertitude, it has been retained as it is the only one for this location until now.

The highest contribution to the helium in the sampled gases comes from the crust, and is higher than 90% in almost all of the samples. A small but significant mantle contribution (2–11%) can be seen in all of the samples collected in the eastern part of the study area from Thermopiles to Ilion (Fig. 9).

3.4. Carbon isotopes

A few samples were analysed for their $\delta^{13}C(CH_4)$ composition (Table 2), displaying a wide range of values (from −50.2 to + 2.5‰). The samples from Amplas and Platystomo ($\delta^{13}C$ from −50.2 to −37.5‰) probably reflect thermogenic gas generation from the burial of the organic-rich flysch of the Pindos zone, which is widespread close to the two localities. The value measured at Archani (−25.4‰) falls in the range typical of abiogenic gas generated by serpentinisation processes in ophiolithic complexes (Etiope et al., 2011, 2013). The values measured in the easternmost samples ($\delta^{13}C$ from −24.1 to +2.5‰) could also be generated by abiogenic processes within the hydrothermal systems (Fiebig et al., 2009; Tassi et al., 2012) although the most positive values might have been significantly affected by methanotrophic consumption. Thick microbial mats, which could explain the biologic oxidation of methane, can be clearly seen at Thermopiles. Methanotrophic consumption cannot be completely ruled out for the other thermal springs as well, but if this is the case changes in their isotopic composition would be more limited due to their higher CH_4 contents. Further measurements, including hydrogen isotopes and $C_2 + C_3$ hydrocarbon contents, are necessary to better constrain the origin of methane in all of these sites.

The isotopic composition of CO_2–C displays a smaller range (from −10.7 to −2.4‰) in respect to that of CH_4–C. The measured range overlaps the typical magmatic CO_2 (−4 to −8‰; Macpherson and Mattey, 1994 and references therein). However, due to the fact that volcanic CO_2 in the Mediterranean region tends to be characterized by relatively elevated $\delta^{13}C$ compositions, the most positive values measured in the study area can also be related to the recent volcanic activity (Parks et al., 2013). The similarities in $\delta^{13}C$ compositions from various Mediterranean volcanoes suggest that this is a regional effect. Carbonate basement is found beneath most of these volcanoes, so it is possible that their unusual $\delta^{13}C(CO_2)$ compositions result from a mixed magmatic-crustal limestone source (e.g., Tassi et al., 2013 and references therein) although contamination of the mantle at depth has also been suggested (e.g., Parello et al., 2000).

The CO_2 vs. $\delta^{13}C$ plot of the samples with CO_2 concentrations above 100,000 μmol/mol (Fig. 10a) shows a positive relationship between the two variables, suggesting the loss of CO_2 through dissolution. Due to the preferential uptake of the heavy carbon in the dissolved phase, the progressive dissolution of CO_2 in the water will therefore progressively reduce the CO_2 concentration and lower the $\delta^{13}C(CO_2)$ in the gas phase. This dissolution process can also be made evident by the relative enrichment in the gas phase of less soluble gases such as N_2 and He (Fig. 10b and c). However, the alignment of samples collected at Edipsos shows another process. The waters at the emerging point are sometimes vigorously bubbling, indicating a high gas pressure within the reservoir. The gas phase in this area probably begins to separate at depth, leaving a dissolved gas phase that is progressively depleted in the less soluble gases (i.e. He and N_2). This residual phase is finally separated from the water at shallow depth or at the emerging point where it has been sampled. This can be seen in Figure 10b and c, where the samples collected at Edipsos are progressively enriched in more soluble CO_2. Both processes can be modelled as open system Rayleigh-type process (Fig. 10d) where the starting gas composition looses either He (Edipsos) or CO_2 (Ipatis, Psoroneria, Thermopiles, Kamena Vourla, Gialtra and Ilion).

Basing on the above considerations, the most representative composition of the gases not affected by shallow processes should

Table 2
Chemical and isotopic composition of the gas sampled in the study area.

	Sample	Date	He ppm	H_2 ppm	O_2 ppm	N_2 ppm	CH_4 ppm	CO_2 ppm	H_2S ppm	Ar ppm	$\partial^{13}C(CO_2)$ ‰ (vs PDB)	$\partial^{13}C(CH_4)$ ‰ (vs PDB)	$\partial^{15}N(N_2)$ ‰ (vs air)	R/R_A	He/Ne	R_C/R_A	Error	$CO_2/^3He$	%Atm	%Rad	%Mag
Amplas	Amplas	07/02/2005	52	<5	1400	116,000	884,000	7000	n.d.	n.d.	−7.3	−37.5	n.d.	n.d.	n.d.	n.a.	n.a.	n.a.	n.a.	n.a.	n.a.
	Amplas	28/03/2008	57	24	600	81,600	915,000	100	n.d.	n.d.	n.d.	−50.2	n.d.	0.048	55.8	0.04	0.001	2.62×10^7	0.5	99.0	0.5
	Amplas	12/10/2008	114	29	<200	161,000	829,000	3500	n.d.	2500	n.d.	n.d.	n.d.	n.d.	n.d.	n.a.	n.a.	n.a.	n.a.	n.a.	n.a.
Platystomo	Platystomo[a]	26/06/2009	103	34	425	852,000	135,000	11,400	n.d.	n.d.	n.d.	−44.7	n.d.	0.102	15.7	0.09	0.002	7.73×10^8	1.8	97.1	1.1
Archani	Archani[a]	28/03/2008	25	<5	4500	969,000	26,700	10	n.d.	n.d.	n.d.	n.d.	n.d.	n.d.	n.d.	n.a.	n.a.	n.a.	n.a.	n.a.	n.a.
	Archani[a]	26/06/2009	60	<5	16,600	946,000	37,700	17	n.d.	n.d.	n.d.	−25.4	n.d.	0.374	0.75	0.02	0.005	5.56×10^5	37.3	62.7	0.0
Ipatis	Ipatis drilling	14/09/2006	74	<5	8400	52400	4600	929000	1400	n.d.	n.d.	n.d.	n.d.	n.d.	n.d.	n.a.	n.a.	n.a.	n.a.	n.a.	n.a.
	Ipatis spa	14/09/2006	139	<5	200	25,400	5400	958,000	2500	n.d.	−5.2	n.d.	n.d.	0.064	974	0.06	0.001	7.67×10^{10}	0.0	99.2	0.8
Psoroneria	Psoroneria 1	12/12/2004	1000	<5	4400	442,000	474	556,000	n.d.	n.d.	−6.2	n.d.	n.d.	n.d.	n.d.	n.a.	n.a.	n.a.	n.a.	n.a.	n.a.
	Psoroneria 1	27/03/2008	827	<5	4000	407,000	612	588,000	n.d.	n.d.	−6.0	n.d.	1.8	0.074	455	0.07	0.003	6.87×10^9	0.0	99.0	1.0
	Psoroneria 1	28/06/2009	763	<5	716	387,000	682	598,000	n.d.	n.d.	−5.8	n.d.	n.d.	0.073	303	0.07	0.003	7.66×10^9	0.1	99.0	1.0
	Psoroneria 1	07/11/2012	908	<5	5700	448,000	919	538,000	n.d.	n.d.	n.d.	n.d.	n.d.	0.076	316	0.07	0.0004	5.60×10^9	0.1	98.9	1.0
	Psoroneria 2	12/12/2004	991	<5	2900	461,000	769	532,000	n.d.	n.d.	−5.9	n.d.	n.d.	n.d.	n.d.	n.a.	n.a.	n.a.	n.a.	n.a.	n.a.
	Psoroneria 2	14/09/2006	526	<5	<200	311,000	742	674,000	n.d.	n.d.	−6.1	n.d.	n.d.	0.077	136	0.07	0.002	1.19×10^{10}	0.2	98.8	1.0
	Psoroneria 2	27/10/2007	835	<5	1900	422,000	1090	563,000	n.d.	3650	−5.8	n.d.	n.d.	0.069	42.3	0.06	0.002	7.01×10^9	0.7	98.5	0.8
	Psoroneria 2	12/02/2008	931	<5	800	442,000	809	546,000	n.d.	n.d.	−5.9	n.d.	n.d.	n.d.	n.d.	n.a.	n.a.	n.a.	n.a.	n.a.	n.a.
	Psoroneria 2	27/03/2008	890	<5	<200	367,000	643	624,000	n.d.	5740	−5.3	n.d.	1.8	0.077	660	0.08	0.003	6.48×10^9	0.0	99.0	1.0
	Psoroneria 3	27/03/2008	763	<5	58,700	348,000	513	570,000	n.d.	n.d.	−5.8	n.d.	n.d.	n.d.	n.d.	n.a.	n.a.	n.a.	n.a.	n.a.	n.a.
Thermopiles	Thermopiles	02/12/2004	237	<5	1500	183,000	846	824,000	n.d.	n.d.	−5.2	n.d.	n.d.	0.176	347	0.18	0.001	1.41×10^{10}	0.1	97.4	2.6
	Thermopiles	10/02/2005	226	<5	<400	141,000	795	853,000	900	n.d.	−5.1	n.d.	n.d.	0.137	144	0.14	0.003	1.96×10^{10}	0.2	97.9	1.9
	Thermopiles	09/04/2005	207	<5	2800	152,000	799	847,000	n.d.	n.d.	−5.5	n.d.	n.d.	0.210	204	0.21	0.002	1.39×10^{10}	0.1	96.8	3.1
	Thermopiles	10/11/2005	210	11	<400	145,000	790	843,000	1700	2670	−5.4	n.d.	n.d.	0.213	269	0.21	0.001	1.35×10^{10}	0.1	96.8	3.1
	Thermopiles	30/01/2006	246	<5	2300	167,000	868	830,000	n.d.	n.d.	−5.9	n.d.	n.d.	n.d.	n.d.	n.a.	n.a.	n.a.	n.a.	n.a.	n.a.
	Thermopiles	25/06/2006	253	<5	<400	150,000	807	850,000	n.d.	n.d.	−5.0	n.d.	n.d.	0.224	161	0.22	0.004	1.07×10^{10}	0.2	96.6	3.3
	Thermopiles	17/07/2006	221	<5	1300	135,000	750	848,000	n.d.	n.d.	−5.1	n.d.	n.d.	0.210	79	0.21	0.003	1.31×10^{10}	0.4	96.6	3.0
	Thermopiles	14/09/2006	168	<5	<400	127,000	710	873,000	n.d.	n.d.	−5.4	n.d.	n.d.	0.233	47	0.23	0.004	1.59×10^{10}	0.6	96.0	3.3
	Thermopiles	21/07/2007	156	<5	<400	125,000	695	871,000	n.d.	1270	−5.7	n.d.	n.d.	0.198	131	0.20	0.003	2.01×10^{10}	0.2	96.9	2.9
	Thermopiles	27/10/2007	207	<5	21,100	204000	738	773,000	n.d.	n.d.	−5.7	n.d.	n.d.	0.202	78	0.20	0.004	1.32×10^{10}	0.4	96.7	2.9
	Thermopiles	12/02/2008	260	<5	3200	169,000	828	808,000	n.d.	n.d.	−6.0	n.d.	n.d.	0.212	259	0.21	0.004	1.05×10^{10}	0.1	96.8	3.1
	Thermopiles	28/03/2008	213	<5	<400	133,000	745	855,000	n.d.	1870	−5.8	n.d.	n.d.	0.170	544	0.17	0.010	1.69×10^{10}	0.0	97.5	2.5
	Thermopiles	28/06/2008	198	<5	2800	156,000	673	835,000	n.d.	n.d.	−6.1	n.d.	n.d.	0.197	943	0.20	0.004	1.53×10^{10}	0.0	97.1	2.9
	Thermopiles	12/10/2008	199	<5	<400	140,000	942	864,000	n.d.	n.d.	−5.6	n.d.	n.d.	0.197	282	0.20	0.010	1.57×10^{10}	0.1	97.0	2.9
	Thermopiles	28/06/2009	216		159	124,000	694	880,000	n.d.	n.d.	−5.5	n.d.	n.d.	0.199	126	0.20	0.005	1.47×10^{10}	0.2	96.9	2.9
	Thermopiles	01/03/2010	235	<5	<400	144,000	741	826,000	n.d.	n.d.	−5.7	n.d.	n.d.	0.245	10	0.22	0.007	1.03×10^{10}	3.1	93.8	3.2
	Thermopiles	26/04/2010	268	<5	<400	200,000	858	774,000	n.d.	n.d.	−5.8	n.d.	n.d.	n.d.	n.d.	n.a.	n.a.	n.a.	n.a.	n.a.	n.a.
	Thermopiles	21/09/2010	234		1400	159,000	787	812,000	n.d.	n.d.	−5.9	−1.5	n.d.	0.216	109	0.21	0.003	1.15×10^{10}	0.3	96.6	3.1
	Thermopiles	17/06/2011	456	38	<400	287,000	990	687,000	n.d.	n.d.	−5.0	n.d.	n.d.	0.233	97	0.23	0.008	4.62×10^9	0.3	96.3	3.4
	Thermopiles	17/02/2012	211	<5	996	140,000	717	835,000	n.d.	n.d.	−5.6	n.d.	n.d.	0.212	95	0.21	0.001	1.33×10^{10}	0.3	96.6	3.1
	Thermopiles	07/11/2012	256		2300	160,000	786	815,000	n.d.	n.d.	−5.9	n.d.	n.d.	0.225	266	0.22	0.001	1.01×10^{10}	0.1	96.6	3.3
Kammena Vourla	Kammena Vourla	02/12/2004	1140	<5	5300	753,000	890	252,000	n.d.	n.d.	−8.4	n.d.	n.d.	0.490	48.1	0.48	0.003	3.22×10^8	0.6	92.1	7.3
	Kammena Vourla	27/03/2008	861	<5	5100	762,000	1780	232,000	n.d.	n.d.	−9.4	n.d.	n.d.	0.485	222	0.48	0.010	3.97×10^8	0.1	92.6	7.3
	Kammena Vourla	28/10/2008	500	<5	31,500	679,000	211	291,000	n.d.	6781	−8.8	n.d.	n.d.	n.d.	n.d.	n.a.	n.a.	n.a.	n.a.	n.a.	n.a.
	Kammena Vourla	25/06/2009	797	<5	1700	693,000	10,000	299,000	n.d.	6180	n.d.	n.d.	1.3	0.515	96.4	0.51	0.006	5.20×10^8	0.3	91.9	7.8
	Kammena Vourla 2	02/12/2004	775	<5	5600	636,000	1070	364,000	n.d.	n.d.	−6.9	n.d.	n.d.	n.d.	n.d.	n.a.	n.a.	n.a.	n.a.	n.a.	n.a.
Gialtra	Gialtra (a)	15/09/2006	248	<5	33,100	873,000	262	93,300	n.d.	n.d.	n.d.	n.d.	n.d.	0.399	16.1	0.39	0.007	6.75×10^8	1.7	92.5	5.7
	Gialtra	29/03/2008	397	<5	39,000	864,000	954	130,000	n.d.	n.d.	−10.7	n.d.	n.d.	0.442	80.6	0.44	0.014	5.29×10^8	0.4	93.0	6.6
	Gialtra	27/06/2009	395	<5	14,600	888,000	1322	100,000	n.d.	9811	n.d.	−9.8	0.5	0.425	41.3	0.42	0.013	4.27×10^8	0.7	93.0	6.3
Edispos	Damaria	12/12/2004	<5	<5	4200	15,200	251	973,000	n.d.	n.d.	−3.1	n.d.	n.d.	n.d.	n.d.	n.a.	n.a.	n.a.	n.a.	n.a.	n.a.
	Damaria	09/11/2005	17	<5	800	17,900	4910	981,000	250	331	−2.6	n.d.	n.d.	0.385	195	0.38	0.002	1.07×10^{11}	0.1	94.1	5.8

(*continued on next page*)

Table 2 (*continued*)

	Sample	Date	He ppm	H_2 ppm	O_2 ppm	N_2 ppm	CH_4 ppm	CO_2 ppm	H_2S ppm	Ar ppm	$\delta^{13}C(CO_2)$ ‰ (vs PDB)	$\delta^{13}C(CH_4)$ ‰ (vs PDB)	$\delta^{15}N(N_2)$ ‰ (vs air)	R/R_A	He/Ne	R_C/R_A	Error	$CO_2/^3He$	%Atm	%Rad	%Mag
	Damaria	29/03/2008	10	<5	2700	21,100	4110	956,000	200	n.d.	−2.4	n.d.	n.d.	0.415	20.1	0.41	0.005	1.65×10^{11}	1.5	92.4	6.0
	Damaria	29/03/2008	1.8	<5	<200	2600	861	991,000	300	69.3	−3.0	n.d.	n.d.	0.423	54.9	0.42	0.005	9.28×10^{11}	0.5	93.2	6.3
	Damaria	27/06/2009	9	<5	417	10,100	3462	979,000	140	n.d.	−2.5	−24.1	2.5	0.346	32.7	0.34	0.005	2.25×10^{11}	0.9	94.0	5.0
	Termopotamos	09/11/2005	0.4	<5	6200	26,500	298	949,000	120	n.d.	−2.9	n.d.	n.d.	0.867	2.3	0.85	0.045	1.97×10^{12}	13.8	75.1	11.1
	Termopotamos	15/09/2006	0.3	5	390	1800	168	991000	n.d.	n.d.	−3.2	n.d.	n.d.	0.427	2.9	0.36	0.034	6.40×10^{12}	11.1	84.2	4.7
	Edispos 3	09/11/2005	<5	<5	800	5100	1210	988,000	n.d.	n.d.	−3.0	n.d.	n.d.	n.d.	n.d.	n.a.	n.a.	n.a.	n.a.	n.a.	n.a.
Ilion	Ilion ([a])	15/09/2006	88	45	23,100	207,000	1250	768,000	n.d.	n.d.	n.d.	n.d.	n.d.	0.354	2.5	0.31	0.005	1.77×10^{10}	11.1	85.3	3.6
	Ilion	29/03/2008	102	<5	800	75,500	1630	919,000	n.d.	n.d.	−2.6	n.d.	n.d.	0.247	341	0.25	0.006	2.60×10^{10}	0.1	96.3	3.6
	Ilion	27/06/2009	103	<5	1600	68,900	1511	900,000	<10	n.d.	n.d.	2.5	1.2	0.281	107	0.28	0.006	2.22×10^{10}	0.3	95.6	4.1

[a] Dissolved gases. n.d. = not determined; n.a. = not applied; %Atm, %Rad and %Mag refer to the source contribution of the atmosphere, crustal radiogenic and mantle to the helium content of the sample (see text for calculation).

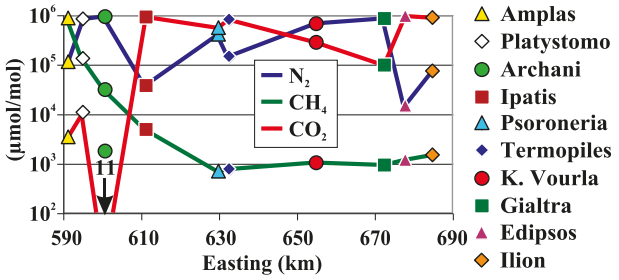

Figure 6. Variations along the study area of the concentrations of the main gases. Only the median values of Nitrogen, Methane and Carbon Dioxide are shown.

have a $\delta^{13}C$ of about $-2.5 \pm 0.5‰$, He concentrations of 10–30 µmol/mol and a $CO_2/^3He$ ratio of 0.8–30 $\times$ 10^{10}. Taking into account the compositions suggested by Sano and Marty (1995) for sediments (*S*), MORB-like mantle (*M*), and limestones (*L*) end-members ($\delta^{13}C(CO_2)$ = −30‰, −5‰ and 0‰; and $CO_2/^3He = 1 \times 10^{13}$, 2×10^9 and 1×10^{13}, for *S*, *M* and *L* respectively), the obtained values correspond to mantle contributions of 1–19%, limestone contributions of 75–93% and sediment contributions of 3–10%. These values are in line with the proportions of the mantle and crustal contributions obtained from the He isotopic composition.

The obtained composition of the deep end-member of CO_2 in the study area falls within the range of values ($\delta^{13}C$ −3.5 – +0.5‰; $CO_2/^3He$ 0.3–90 10^{10}) measured along the SAAVA (D'Alessandro et al., 2010; Parks et al., 2013 and references therein). These values were explained by decarbonation of marine limestone within the crust (Parks et al., 2013). Limestone is also widespread in the sedimentary sequences of the studied area, indicating that the CO_2 has a similar origin. Assuming a minimum temperature of 400 °C for the metamorphic decarbonation reactions that liberate CO_2 (Ferry, 1991) and a thermal gradient of >50 °C/km (Metaxas et al., 2010; Karastathis et al., 2011), the CO_2 should originate at a depth <8 km.

3.5. Variations in fluid geochemistry along the graben

The graphs in Figures 6 and 11 reveal clear geographical trends in the measured parameters. The increase of water salinity (Fig. 11c) is due to the seawater contamination of the hydrothermal system. The sites of Kammena Vourla, Gialtra, Edipsos and Ilion lie within about 100 m from the coast, thereby explaining the seawater

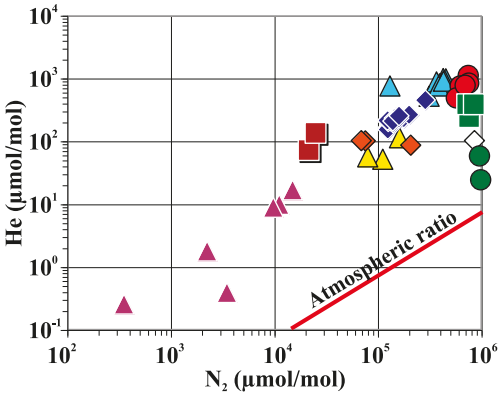

Figure 7. He–N_2 binary plot of the gas samples collected in the study area. In red the He/N_2 ratio in the atmosphere. (For interpretation of the references to colour in this figure legend, the reader is referred to the web version of this article.)

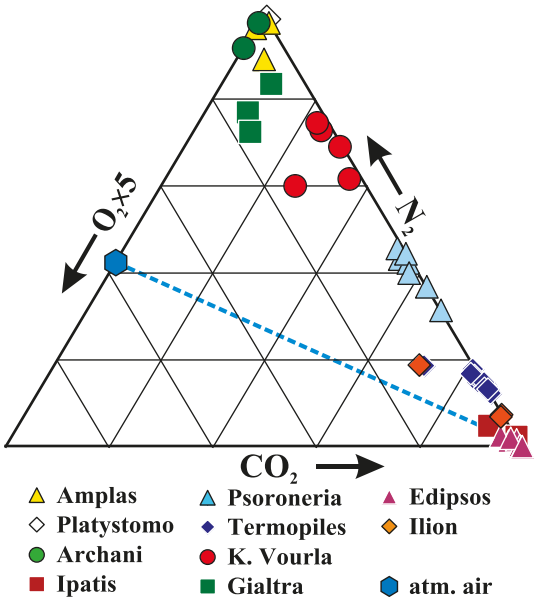

Figure 8. O_2–N_2–CO_2 triangular plot. The dashed line represents the O_2/N_2 ratio in atmospheric air.

contamination. The sites of Ipatis, Psoroneria and Thermopiles are presently at greater distances from the coast (23, 6 and 5 km respectively). But they were much closer to the sea in the recent geological past due to variations in sea level as well as the progradation of the Sperchios river delta. Paleogeographical information indicates that Ipatis was located less than 10 km from the sea 4500 years BP, and historical accounts tell us that until the beginning of the 19th century the coast close to Psoroneria and Termopiles corresponded to that existing in 480 BC when the spring

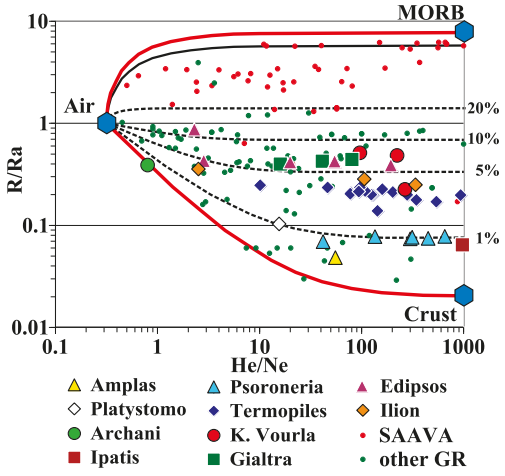

Figure 9. Helium isotope signature of the collected samples. Data are superimposed on mixing curves (in red) of three end-member components (MORB-type mantle $R/R_A = 8$ and $^4He/^{22}Ne > 1000$, crust $R/R_A = 0.02$ and $^4He/^{22}Ne > 1000$, and air $R/R_A = 1$ and $^4He/^{22}Ne \approx 3$). Further mixing curves between air and deep fluids with 1, 5, 10 and 20% mantle contribution have also been added. The mantle contribution has been calculated considering the European SCLM-type mantle with $R/R_A = 6.3$ (black line). Literature data of samples collected along the entire Greek territory has also been displayed for comparison (Shimizu et al., 2005; Pik and Marty, 2009; D'Alessandro et al., 2008, 2010; INGV-Pa unpublished database). These samples has been subdivided in a first subgroup collected along the South Aegean Active Volcanic Arc (SAAVA) and second subgroup collected along the remaining Greek territory. (For interpretation of the references to colour in this figure legend, the reader is referred to the web version of this article.)

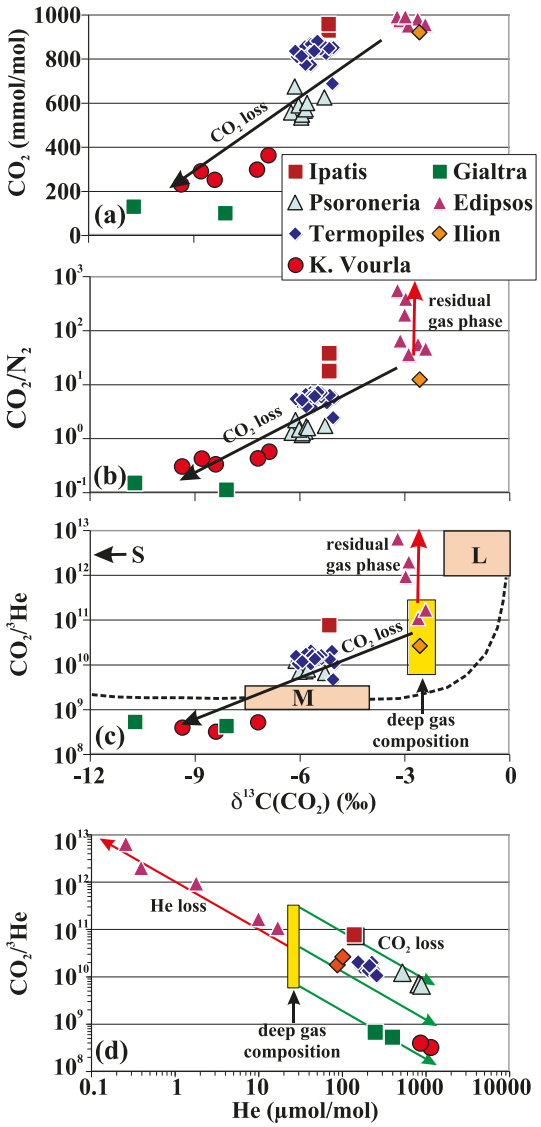

Figure 10. (a) CO_2–$\delta^{13}C(CO_2)$, (b) CO_2/N_2–$\delta^{13}C(CO_2)$, (c) $CO_2/^3He$–$\delta^{13}C(CO_2)$ and (d) $CO_2/^3He$–He plots. In a, b and c the black arrows evidence the CO_2 loss due to dissolution in the liquid phase, while the red arrows show the evolution of the residual gas phase due to gas exsolution. In c the end-member compositions for sediments (*S*), MORB-like mantle (*M*) and limestones (*L*) are $\delta^{13}C(CO_2) = -30‰$, $-5‰$ and $0‰$; and $CO_2/^3He = 1 \times 10^{13}$, 2×10^9 and 1×10^{13}, respectively (Sano and Marty, 1995) and the dashed lines represent the mixing paths between the end-members. In c and d the yellow area shows the extrapolated compositional range of the gas not modified by shallow processes. In d the red arrow shows the gas evolution due to He loss while the green arrows that due to CO_2 loss both along open system Rayleigh-type paths. (For interpretation of the references to colour in this figure legend, the reader is referred to the web version of this article.)

discharged a few tens of metres from the sea (Kraft et al., 1987), thereby accounting for the seawater intrusion that also exists at these sites.

The temperature of the hydrothermal manifestations increases from <30 °C in the west up to >60 °C in the east (Fig. 11b) indicating a progressively higher heat flux going east along the graben.

The helium isotopic compositions distinguish the westernmost sites where the helium shows an almost pure crustal origin from the easternmost sites with a small but significant mantle contribution (Fig. 11a). This contribution could have been the direct result of tectonic structures that cut the whole crust and reached the mantle, as has been demonstrated for continental strike-slip faults

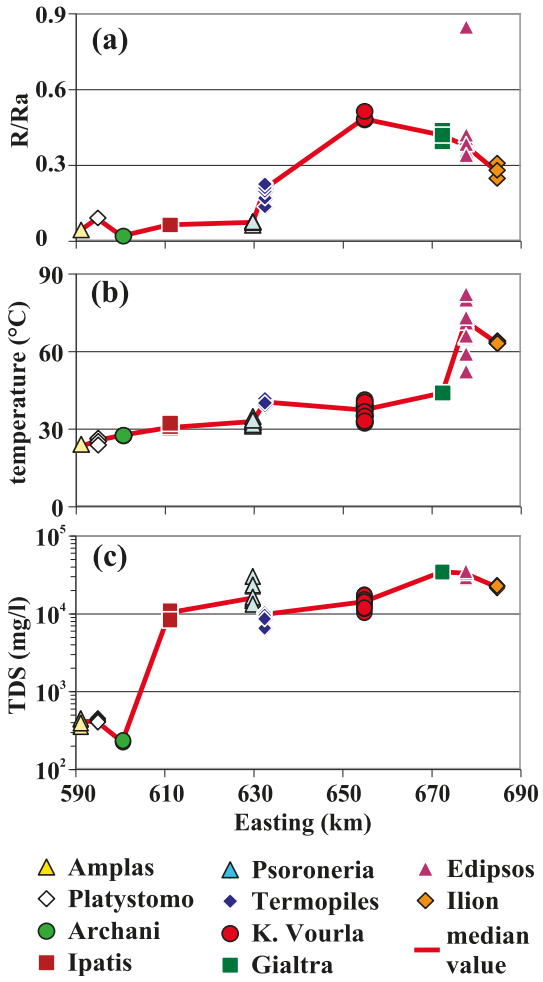

Figure 11. Variations along the study area of the concentrations of the R/R_A values (a), the water temperature (b) and the (TDS) total dissolved solids (c) in the collected waters. The red line evidences the variation of the median value along the basin. (For interpretation of the references to colour in this figure legend, the reader is referred to the web version of this article.)

like that of the San Andreas fault (Kulongoski et al., 2013) and the North Anatolian fault (NAF; Gülec et al., 2002), contributing to the fluids discharged at a distance up to about 30 km from the fault. The tectonic structures bordering the studied area do not have these characteristics and do not provide this kind of pathway for mantle fluids. The above-mentioned NAF, whose westernmost termination is thought to reach the rift in the Maliakos bay area through the Orei channel (Fig. 1), could represent the connection to the mantle. The sites with a distinct mantle contribution are all found at a distance of less than 10 km from tectonic structures related to the western termination of the NAF system. Until now, no study has demonstrated that the NAF reaches the base of the crust in the study area therefore this hypothesis is speculative at this point. However, the NAF and the other extensive fault systems of the area have facilitated the upraise of magma batches that have sometimes erupted at the surface during the recent past. Karastathis et al. (2011) found a large area below the North Evian Gulf with temperatures above the Curie point (>560 °C) at a depth of 7–8 km in correspondence with low seismic P-wave velocity values and high Poisson ratios, attributing them to the presence of molten magma. The latter could be the source of both the heat that sustains the hydrothermal systems and the mantle component of He and CO_2 in the emitted gases.

Pik and Marty (2009) have shown that both the Corinth graben and the Sprechios basin – Northern Evoikos Gulf graben share similar pattern of He origin along with an analogous tectonic regime. In both areas in the western part, excluding atmospheric contributions, He has an almost exclusively crustal origin while in the eastern part a mantle contribution is evident. Although the data used by Pik and Marty (2009) for the Sprechios basin – Northern Evoikos Gulf graben taken from the previously unpublished University of Cambridge He database were incomplete and sometimes wrong, the present study confirms this pattern. The authors attributed the mantle contribution in the eastern part of both grabens to the "magmatic signature of the arc fluids" (Pik and Marty, 2009) and indeed the highest values are always closely related to recent (Quaternary) or even active volcanic systems.

4. Conclusions

The complex geodynamic setting of the studied area is clearly reflected in the wide compositional range of both the waters and the gases collected from the thermal manifestations showing contributions from various sources. On the basis of their water composition, they can be roughly subdivided into low-salinity waters (TDS < 0.5 g/l; the three westernmost manifestations) and high-salinity waters (TDS 9 – 35 g/l; the remaining manifestations). The Sodium-Chloride composition of the high-salinity waters can be explained by the mixing of a meteoric low-salinity end-member with seawater. The latter has been partially modified within the hydrothermal systems, sometimes attaining water–rock interaction conditions close to equilibrium. The highest estimated temperatures in the reservoirs fall within a range of 150–170 °C.

The low-salinity waters display a wider compositional range then waters close to the local cold groundwater (Platystomo), which has sometimes been modified by solid phase precipitation (Amplas). The most peculiar low-salinity water is that collected at Archani; regarding CO_2 (high pH, very low Mg and TDC), it shows features typical of water that has been equilibrated in an ophiolithic aquifer in closed conditions.

The gas composition is more complicated than the water composition, and does not allow a simple subdivision of the manifestations to be made. Instead, it reveals multiple sources (atmosphere, crust, mantle and hydrothermal systems). The dominating gases are CH_4 (Amplas), N_2 (Platystomo, Archani, Psoroneria, Kamena Vourla and Gialtra) and CO_2 (Ipatis, Thermopiles, Edipsos and Ilion). The isotope composition of CH_4 indicates a thermogenic origin in the westernmost sites and a hydrothermal origin (possibly abiogenic) in the easternmost ones. Methane at Archani indicates an abiogenic origin typical of ophiolithe-related hyperalkaline waters.

As shown by the N_2/Ar ratios, N_2 has a prevailing atmospheric origin although a contribution of crustal nitrogen is indicated by slightly positive $\delta^{15}N$ (+0.5 to +2.5‰).

The concentrations and isotope composition of CO_2 in the manifestations are strongly affected by dissolution processes and the $\delta^{13}C$ of the deep end-member has been estimated to be about −2.5‰. This value falls within the range measured in the volcanic systems of the South Aegean Active Volcanic Arc and can be similarly interpreted as a mixing between CO_2 of mantle origin with CO_2 deriving from marine carbonate thermal metamorphism.

In contrast to the main chemical composition of the gases, the manifestations can be clearly subdivided according to the He isotopic composition, with the westernmost ones showing an almost pure crustal origin (<0.1 R_C/R_A) and the easternmost ones having a low but significant mantle contribution (up to 0.85 R_C/R_A). This mantle contribution could be attributed to the upraise from the mantle through a continental strike slip fault like the North

Anatolian fault whose western termination reaches the studied area. Alternatively, it could have been derived from magma batches that have been detected at shallow depths (~8 km) within the crust in the Northern Evoikos Gulf, which could also provide the necessary heat to sustain the hydrothermal systems of the area.

Acknowledgements

The insightful comments of Franco Tassi and two anonymous referees and of the guest editor Antonio Caracausi helped us to improve the manuscript.

Appendix A. Supplementary data

Supplementary data related to this article can be found at http://dx.doi.org/10.1016/j.marpetgeo.2013.12.011.

Appendix A

Brief description of the thermal manifestations

Going from west to east 10 groups of thermal manifestations can be recognised along the graben: Amplas, Platystomo, Archani, Ipatis, Psoroneria, Thermopiles, Kamena Vourla, Gialtra, Edipsos and Ilion (Fig. 1). All of these manifestations emerge in close connection to one of the tectonic structures that border the graben.

Amplas, also known as Paleovracha, is a low flow spring (~1 l/s) forming a small pond in which gases are gently bubbling. The waters, pumped from a shallow well, are exploited by a small thermal bath.

At Platystomo at least three groups of springs emerge at distances of about 100 m from each other. Two of them are free flowing being close to abandoned thermal baths while the third one is exploited by a spa. The total water yield is about 10 l/s. No free gases were found during our campaigns but Minissale et al. (1989) published the analysis of a free gas sample.

Archani is a small spring with a low water flux (~2 l/s) issuing along a creek in an area of serpentinised ophiolites. The spring was once exploited by a small thermal bath which is nowadays abandoned. No bubbling gases are present.

Ipatis is a small village built around its thermal spring, which is exploited by a big thermal bath. The water yield is about 10 l/s and at the water outlet gas is vigorously bubbling. At about 500 m from the main spring in SW direction a drilling reached at unknown depth the thermal aquifer. Local people use the low artesian flow (<1 l/s) for bathing their feet. Sometimes during wet periods, gases are bubbling in the ponds that form around the well.

Psoroneria, also known as Damasta, is a 400 m wide area with three main groups of thermal springs with a total yield of >30 l/s. The springs form wide pools were abundant gases are bubbling. The sites were rudimentarily equipped with stairs and handrails and are widely used for free open-air bathing.

Thermopiles is a spring that forms a large pool (10 m diameter) with abundant gas bubbling whose outlet is drained by a channel that brings the water to the seashore. Active travertine deposition takes place along the channel (Kanellopoulos, 2012). The nearby thermal baths are nowadays abandoned but people used to take a bath both in the pool at the spring and in another pool that forms after a small waterfall along the channel.

Kamena Vourla is an important tourist destination on the Northern Evoikos Gulf coast and the thermal springs are one of its main attractions. Two groups of thermal springs are recognisable, one within the small town and the other, also known as Koniavitou, at its north-western outskirts. Only in the first group gases are sometimes sluggishly bubbling.

Gialtra is a small thermal area where two spring with low yields (<1 l/s) issue a few tens of metres from the sea-shore. The water is used by a small thermal bath and at the spring outlets gases bubble sluggishly.

Loutra Edipsos is one of the major spa towns in Greece. Up to 65 springs has been recognised over an area of about 0.3 km^2, clustering in 13 main groups with temperatures ranging from 35 to 83 °C (Margomenou-Leonidopoulou, 1976). Most of the springs are exploited by numerous thermal bath facilities. The total yield has been estimated in 100 l/s. At most of the springs, gases are vigorously bubbling in the water and there is widespread active travertine deposition (Kanellopoulos, 2012). Travertine outcrops form often thick deposits sometimes exploited as building material.

Ilion is a thermal spring issuing less 10 m from the sea-shore with a yield of about 5 l/s and abundant bubbling gases. It is used for open-air bathing at the sea-shore where the thermal water mixes with sea-water.

References

Allard, P., Jean-Baptist, P., D'Alessandro, W., Parello, F., Parisi, B., Flehoc, C., 1997. Mantle derived helium and carbon in groundwaters and gases of Mount Etna, Italy. Earth Planet. Sci. Lett. 148, 501–516. http://dx.doi.org/10.1016/S0012-821X(97)00052-6.

Antonopoulos, J., 1992. The tsunami of 426 BC in the Maliakos Gulf, Eastern Greece. Nat. Hazards 5, 83–93.

Ballentine, C.J., Burnard, P.G., 2002. Production, release and transport of noble gases in the continental crust. Rev. Mineral. Geochem. 47, 481–538.

Ballentine, C.J., Burgess, R., Marty, B., 2002. Tracing fluid origin, transport and interaction in the crust. Rev. Mineral. Geochem. 47, 539–614. http://dx.doi.org/10.2138/rmg.2002.47.13.

Barnes, I., Leonis, C., Papastamataki, A., 1986. Stable isotope tracing of the origin of CO_2 discharges in Greece. In: Proceedings of the 5th International Symposium on Underground Water Tracing, Athens, pp. 25–42.

Bellon, H., Jarrige, J.J., Sorel, D., 1979. Les activites magmatiques egeennes de l'oligocene a nos jours et leurs cadres geodynamiques. Donnees nouvelles et synthese. Rev. Geol. Dyn. Geogr. Phys. 21, 41–55.

Bornovas, J., Rondogianni-Tsiambaou, Th, 1983. Geological Map of Greece, 1: 500,000. Institute of Geology and Mineral Exploration, (IGME), Athens.

Burton, P.W., Xu, Y., Qin, C., Tselentis, G., Sokos, E., 2004. A catalogue of seismicity in Greece and the adjacent areas for the twentieth century. Tectonophysics 390, 117–127. http://dx.doi.org/10.1016/j.tecto.2004.03.020.

Capasso, G., Favara, R., Grassa, F., Inguaggiato, S., Longo, M., 2005. On-line technique for preparation and measuring stable carbon isotope of total dissolved inorganic carbon in water samples ($\delta^{13}C_{TDIC}$). Ann. Geophys. 48, 159–166.

Cipolli, F., Gambardella, B., Marini, L., Ottonello, G., Zuccolini, M.V., 2004. Geochemistry of high-pH waters from serpentinites of the Gruppo di Voltri (Genova, Italy) and reaction path modeling of CO_2 sequestration in serpentinite aquifers. Appl. Geochem. 19, 787–802.

Craig, H., 1961. Isotopic variations in meteoric waters. Science 133, 1702–1703.

D'Alessandro, W., Brusca, L., Kyriakopoulos, K., Michas, G., Papadakis, G., 2008. Methana, the westernmost active volcanic system of the south Aegean arc (Greece): insight from fluids geochemistry. J. Volcanol. Geotherm. Res. 178, 818–828. http://dx.doi.org/10.1016/j.jvolgeores.2008.09.014.

D'Alessandro, W., Brusca, L., Martelli, M., Rizzo, A., Kyriakopoulos, K., 2010. Geochemical characterization of natural gas manifestations in Greece. In: Proceedings of the 12th International Congress of the Geological Society of Greece, Patras, May, 2010. Bulletin of the Geological Society of Greece 43/5, pp. 2327–2337. http://www.earth-prints.org/handle/2122/6030.

D'Alessandro, W., Katsanou, K., Lambrakis, N., Bellomo, S., Brusca, L., Liotta, M., 2013. Chemical and isotopic characterisation of bulk deposition in the Louros Basin (Epirus, Greece). Atmos. Res. 132–133, 399–410. http://dx.doi.org/10.1016/j.atmosres.2013.07.007.

Dotsika, E., Lykoudis, S., Poutoukis, D., 2010. Spatial distribution of the isotopic composition of precipitation and spring water in Greece. Global Planet. Change 71, 141–149. http://dx.doi.org/10.1016/j.gloplacha.2009.10.007.

Dunai, T.J., Baur, H., 1995. Helium, neon, and argon systematics of the European subcontinental mantle: implications for its geochemical evolution. Geochim. Cosmochim. Acta 59, 2767–2783.

Duriez, A., Marlin, C., Dotsika, E., Massault, M., Noret, A., Morel, J.L., 2008. Geochemical evidence of seawater intrusion into a coastal geothermal field of central Greece: example of the Thermopylae system. Environ. Geol. 54, 551–564. http://dx.doi.org/10.1007/s00254-007-0857-9.

Etiope, G., Schoell, M., Hosgörmez, H., 2011. Abiotic methane flux from the Chimaera seep and Tekirova ophiolites (Turkey): understanding gas exhalation from low temperature serpentinization and implications for Mars. Earth Planet. Sci. Lett. 310, 96–104. http://dx.doi.org/10.1016/j.epsl.2011.08.001.

Etiope, G., Tsikouras, B., Kordella, S., Ifandi, E., Christodoulou, D., Papatheodorou, G., 2013. Methane flux and origin in the Othrys ophiolite hyperalkaline springs,

Greece. Chem. Geol. 347, 161–174. http://dx.doi.org/10.1016/j.chemgeo.2013.04.003.
Ferry, J.M., 1991. Dehydration and decarbonation reactions as a record of fluid infiltration, in Contact Metamorphism. Rev. Mineral. Geochem. 26, 351–393.
Fiebig, J., Woodland, A.B., D'Alessandro, W., Püttmann, W., 2009. Excess methane in hydrothermal emissions is abiogenic. Geology 37, 495–498.
Fournier, R.O., 1977. Chemical geothermometers and mixing models for geothermal systems. Geothermics 5, 41–50.
Fytikas, M., Kolios, N., 1979. Preliminary heat flow map of Greece. In: Cermak, V., Rybach, L. (Eds.), Terrestrial Heat Flow in Europe. Springer-Verlag, pp. 197–205.
Fytikas, M., Giuliani, O., Innocenti, F., Marinelli, G., Mazzuoli, R., 1976. Geochronological data on recent magmatism of the Aegean Sea. Tectonophysics 31, T29–T34.
Fytikas, M., Margomenou-Leonidopoulou, G., Cataldi, R., 1999. Geothermal Energy in Ancient Greece: From Mythology to Late Antiquity. In: Stories from a Heated Earth. Geothermal Resources Council and IGA, California.
Garagunis, N., 1978. Hydrogeologische Untersuchengen der Thermal- und Mineralquellen im östlichen Mittelgriechenland. Steir. Beiträge Hydrogeol. 30, 5–82.
Gartzos, E., Stamatis, G., 1996. Genesis of the thermal springs of Sperchios graben, Greece. Neues Jahrb. Geol. Palaontol. H2, 91–115.
Gat, J.R., Carmi, I., 1970. Evolution of the isotopic composition of the atmospheric water in the Mediterranean Sea area. J. Geophys. Res. 75, 3039–3048.
Gautheron, C., Moreira, M., Allegre, C., 2005. He, Ne and Ar composition of the European lithospheric mantle. Chem. Geol. 217, 97–112. http://dx.doi.org/10.1016/j.chemgeo.2004.12.009.
Giggenbach, W.F., Corrales, R.S., 1992. The isotopic and chemical composition of waters and steam discharges from volcanic–magmatic-hydrothermal systems of the Guanacoste Geothermal Province. Costa Rica. Appl. Geochem. 7, 309–322.
Gülec, N., Hilton, D.R., Mutlu, H., 2002. Helium isotope variations in Turkey: relationship to tectonics, volcanism and recent seismic activities. Chem. Geol. 187, 129–142.
Inguaggiato, S., Rizzo, A., 2004. Dissolved helium isotope ratios in groundwaters: a new technique based on gas–water re-equilibration and its application to Stromboli volcanic system. Appl. Geochem. 19, 665–673. http://dx.doi.org/10.1016/j.apgeochem.2003.10.009.
Innocenti, F., Agostini, S., Doglioni, C., Manetti, P., Tonarini, S., 2010. Geodynamic evolution of the Aegean: constraints from the Plio-Pleistocene volcanism of the Volos-Evia area. J. Geol. Soc. Lond. 167, 475–489. http://dx.doi.org/10.1144/0016-76492009-149.
Kanellopoulos, C., 2012. Distribution, lithotypes and mineralogical study of newly formed thermogenic travertines in Northern Euboea and Eastern Central Greece. Central Eur. J. Geosci. 4 (4), 545–560. http://dx.doi.org/10.2478/s13533-012-0105-z.
Karastathis, V.K., Papoulia, J., Di Fiore, B., Makris, J., Tsambas, A., Stampolidis, A., Papadopoulos, G.A., 2011. Deep structure investigations of the geothermal field of the North Euboean Gulf, Greece, using 3-D local earthquake tomography and Curie Point Depth analysis. J. Volcanol. Geotherm. Res. 206, 106–120. http://dx.doi.org/10.1016/j.jvolgeores.2011.06.008.
Kelepertsis, A., Tziritis, E., Kelepertsis, E., Leontakianakos, K.P., 2009. Hydrogeochemical characteristics and genetic implications of Edipsos thermal springs, north Euboea, Greece. Central Eur. J. Geosci. 1 (3), 241–250. http://dx.doi.org/10.2478/v10085-009-0019-2.
Kilias, A.A., Tranos, M.D., Papadimitriou, E.E., Karakostas, V.G., 2008. The recent crustal deformation of the Hellenic orogen in Central Greece; the Kremasta and Sperchios Fault Systems and their relationship with the adjacent large structural features. Z. Dtsch. Ges. Geowiss. 159 (3), 533–547. http://dx.doi.org/10.1127/1860-1804/2008/0159-0533.
Klemperer, S.L., Kennedy, B.M., Sastry, S.R., Makovsky, Y., Harinarayana, T., Leech, M.L., 2013. Mantle fluids in the Karakoram fault: helium isotope evidence. Earth Planet. Sci. Lett. 366, 59–70. http://dx.doi.org/10.1016/j.epsl.2013.01.013.
Kraft, J.C., Rapp, G., Szemler, G.J., Tziavos, C., Kase, E.W., 1987. The pass at Thermopylae, Greece. J. Field Archaeol. 14, 181–198.
Kulongoski, J.T., Hilton, D.R., Barry, P.H., Esser, B.K., Hillegonds, D., Belitz, K., 2013. Volatile fluxes through the Big Bend section of the San Andreas Fault, California: helium and carbon-dioxide systematics. Chem. Geol. 339, 92–102. http://dx.doi.org/10.1016/j.chemgeo.2012.09.007.
Lambrakis, N., Kallergis, G., 2005. Contribution to the study of Greek thermal springs: hydrogeological and hydrochemical characteristics and origin of the thermal waters. Hydrogeol. J. 13, 506–521. http://dx.doi.org/10.1007/s10040-004-0349-x.
Lambrakis, N., Zagana, E., Katsanou, K., 2013. Geochemical patterns and origin of alkaline thermal waters in Central Greece (Platystomo and Smokovo areas). Environ. Earth Sci. 69, 2475–2486. http://dx.doi.org/10.1007/s12665-012-2073-5.
Liotta, M., Martelli, M., 2012. Dissolved gases in brackish thermal waters: an improved analytical method. Geofluids 12, 236–244. http://dx.doi.org/10.1111/j.1468-8123.2012.00365.x.
Macpherson, C.G., Mattey, D.P., 1994. Carbon isotope variations of CO_2 in Lau Basin basalts and ferrobasalts. Earth Planet. Sci. Lett. 121, 263–276.
Makris, J., Papoulia, J., Papanikolaou, D., Stavrakakis, G., 2001. Thinned continental crust below northern Evoikos Gulf, central Greece, detected from deep seismic soundings. Tectonophysics 341, 225–236.
Margomenou-Leonidopoulou, G., October 1976. Preliminary report of the research of Aidipsos thermometallic waters. In: Proc. of the International Congress on Thermal Waters. Geothermal Energy and Volcanism of the Mediterranean area, Athens, pp. 340–351.
Metaxas, A., Varvarousis, G., Karydakis, G., Dotsika, E., Papanikolaou, G., 2010. In: Proceedings of the 12th International Congress of the Geological Society of Greece, Patras, May, 2010. Bulletin of the Geological Society of Greece 43/5, pp. 2265–2273.
Minissale, A., Duchi, V., Kolios, N., Totaro, G., 1989. Geochemical characteristics of Greek thermal springs. J. Volcanol. Geotherm. Res. 39, 1–16.
Papadopoulos, G.A., 1982. Active Deep Tectonics of the Aegean and Surrounding Area (Ph D. thesis). University of Thessaloniki (in Greek).
Papadopoulos, G.A., 1989. Seismic and volcanic activities and aseismic movements as plate motion components in the Aegean area. Tectonophysics 167, 31–39.
Papazachos, B., Papazachos, C., 1997. Earthquakes in Greece. Editions Ziti, Thessaloniki.
Papoulia, J., Makris, J., Drakopoulou, V., 2006. Local seismic array observations at north Evoikos, central Greece, delineate crustal deformation between the North Aegean Trough and Corinthiakos Rift. Tectonophysics 423, 97–106. http://dx.doi.org/10.1016/j.tecto.2006.03.021.
Parello, F., Allard, P., D'Alessandro, W., Federico, C., Jean-Baptiste, P., Catani, O., 2000. Isotope geochemistry of Pantelleria volcanic fluids, Sicily Channel rift: a mantle volatile end-member for volcanism in southern Europe. Earth Planet. Sci. Lett. 180, 325–339. http://dx.doi.org/10.1016/S0012-821X(00)00183-7.
Parks, M.M., Caliro, S., Chiodini, G., Pyle, D.M., Mather, T.A., Berlo, K., Edmonds, M., Biggs, J., Nomikou, P., Raptakis, C., 2013. Distinguishing contributions to diffuse CO_2 emissions in volcanic areas from magmatic degassing and thermal decarbonation using soil gas ^{222}Rn–$\delta^{13}C$ systematics: application to Santorini volcano, Greece. Earth Planet. Sci. Lett. 377–378, 180–190. doi.org/10.1016/j.epsl.2013.06.046.
Pe-Piper, G., Piper, J.W., 1989. Spatial and temporal variation in Late Cenozoic back-arc volcanic rocks, Aegean Sea Region. Tectonophysics 169, 113–134.
Pe-Piper, G., Piper, D.J.W., 2002. The Igneous Rocks of Greece. Borntraeger, Stuttgart, 645 pp.
Pertessis, M., 1937. Thermomineral Springs of Greece. In: Publication of the Geological Survey of Greece, n. 24. Athens (in Greek).
Pertessis, M., 1961. Relations entre la composition chimique des sources thermominerales en Grece et la constitution geologique du pays. In: Groundwater in arid zones – Symposium of Athens 10–18 Sep. 1961. IAHS Redbooks 57, pp. 651–656.
Pik, R., Marty, B., 2009. Helium isotopic signature of modern and fossil fluids associated with the Corinth rift fault zone (Greece): implication for fault connectivity in the lower crust. Chem. Geol. 266, 67–75. http://dx.doi.org/10.1016/j.chemgeo.2008.09.024.
Roberts, S., Jackson, J., 1991. Active Normal Faults in Central Greece: an Overview. In: Geological Society London Special Publication 56, pp. 125–142.
Sano, Y., Wakita, H., 1985. Geographical distribution of $^3He/^4He$ in Japan: implications for arc tectonics and incipient magmatism. J. Geophys. Res. 90, 8729–8741.
Sano, Y., Marty, B., 1995. Origin of carbon in fumarolic gas from island arcs. Chem. Geol. 119, 265–274.
Shimizu, A., Sumino, H., Nagao, K., Notsu, K., Mitropoulos, P., 2005. Variation in noble gas isotopic composition of gas samples from the Aegean arc, Greece. J. Volcanol. Geotherm. Res. 140, 321–339. http://dx.doi.org/10.1016/j.jvolgeores.2004.08.016.
Tassi, F., Fiebig, J., Vaselli, O., Nocentini, M., 2012. Origins of methane discharging from volcanic-hydrothermal, geothermal and cold emissions in Italy. Chem. Geol. 310–311, 36–48. http://dx.doi.org/10.1016/j.chemgeo.2012.03.018.
Tassi, F., Vaselli, O., Papzachos, C.B., Giannini, L., Chiodini, G., Vougioukalakis, G.E., Karagianni, E., Vamvakaris, D., Panagiotopoulos, D., 2013. Geochemical and isotopic changes in the fumarolic and submerged gas discharges during the 2011–2012 unrest at Santorini caldera (Greece). Bull. Volcanol. 75. http://dx.doi.org/10.1007/s00445-013-0711-8.
Torfstein, A., Hammerschmidt, K., Friedrichsen, H., Starinsky, A., Garfunkel, Z., Kolodny, Y., 2013. Helium isotopes in Dead sea transform waters. Chem. Geol. 352, 188–201. http://dx.doi.org/10.1016/j.chemgeo.2013.06.008.